2016

Leveraging the information content of process-based models using Differential Evolution and the Extended Kalman Filter

Lucas Howard
University of Vermont

LEVERAGING THE INFORMATION CONTENT OF PROCESS-BASED MODELS USING DIFFERENTIAL EVOLUTION AND THE EXTENDED KALMAN FILTER

A Thesis Presented

by

Lucas J. Howard

to

The Faculty of the Graduate College

of

The University of Vermont

In Partial Fulfillment of the Requirements
for the Degree of Master of Science
Specializing in Civil and Environmental Engineering
May, 2016

Defense Date: March 28, 2016
Thesis Defense Examination Committee:

Donna M. Rizzo, Ph.D., Advisor
Dryver R. Huston, Ph.D., Chairperson
Mandar M. Dewoolkar, Ph.D., P.E.
Cynthia J. Forehand, Ph.D., Dean of the Graduate College

Abstract

Process-based models are used in a diverse array of fields, including environmental engineering to provide supporting information to engineers, policymakers and stakeholdes. Recent advances in remote sensing and data storage technology have provided opportunities for improving the application of process-based models and visualizing data, but also present new challenges. The availability of larger quantities of data may allow models to be constructed and calibrated in a more thorough and precise manner, but depending on the type and volume of data, it is not always clear how to incorporate the information content of these data into a coherent modeling framework. In this context, using process-based models in new ways to provide decision support or to produce more complete and flexible predictive tools is a key task in the modern data-rich engineering world. In standard usage, models can be used for simulating specific scenarios; they can also be used as part of an automated design optimization algorithm to provide decision support or in a data-assimilation framework to incorporate the information content of ongoing measurements. In that vein, this thesis presents and demonstrates extensions and refinements to leverage the best of what process-based models offer using Differential Evolution (DE) the Extended Kalman Filter (EKF).

Coupling multi-objective optimization to a process-based model may provide valuable information provided an objective function is constructed appropriately to reflect the multi-objective problem and constraints. That, in turn, requires weighting two or more competing objectives in the early stages of an analysis. The methodology proposed here relaxes that requirement by framing the model optimization as a sensitivity analysis. For demonstration, this is implemented using a surface water model (HEC-RAS) and the impact of floodplain access up and downstream of a fixed bridge on bridge scour is analyzed. DE, an evoutionary global optimization algorithm, is wrapped around a calibrated HEC-RAS model. Multiple objective functions, representing different relative weighting of two objectives, are used; the resulting rank-orders of river reach locations by floodplain access sensitivity are consistent across these multiple functions.

To extend the applicability of data assimilation methods, this thesis proposes relaxing the requirement that the model be calibrated (provided the parameters are still within physically defensible ranges) before performing assimilation. The model is then dynamically calibrated to new state estimates, which depend on the behavior of the model. Feasibility is demonstrated using the EKF and a synthetic dataset of pendulum motion. The dynamic calibration method reduces the variance of prediction errors compared to measurement errors using an initially uncalibrated model and produces estimates of calibration parameters that converge to the true values. The potential application of the dynamic calibration method to river sediment transport modeling is proposed in detail, including a method for automated calibration using sediment grain size distribution as a calibration parameter.

Acknowledgments

As is inevitably the case with research (and with life), finishing this thesis has come in fits and starts. I have gone from despairing about its contents to being over the moon with a breakthrough, sometimes on the same day. It is natural to feel some pride and sense of achievment when completing something of this nature, and I do feel those things, but my pride is dwarfed by how fortunate I feel to have had the support, trust and belief of countless people. I am very much aware that the chain of events leading me here is more tenuous in actuality than in hindsight, and I have so, so many people to thank for its actualization.

Donna Rizzo, for powering through countless (and embarrassingly poorly proof-read) drafts, given me the guidance and structure that I needed when I needed it in my writing and in general, and inevitably turning two-minute drop-ins into fascinating 45 minute conversations on science and life. I really couldn't have had a better person to work with these past two years. John Hanley, for his wit, skepticism, sense of humor, and consistent frustration with the state of academia. Scott Hamshaw, for his uncomplaining hours spent collecting data for my research and for being the official emergency seminar speaker. Kristen Underwood, who in addition to having an intimidating and encyclopedic knowledge of all things sediment, surface water and geomorphologic, is one of the most genuinely kind and generous people I have had the privilege to meet. Mandar Dewoolkar, for funding me on one of his grants and for helping us push this thesis across the finish line. I would also be remiss if I didn't thank Jordan Duffy, Alex Morton and Kira Kelley for their time and efforts in the service of what turned out to be a frustrating cause.

Going back in time a little bit, thank you to Dan Nachman for imposing his friendship on Charlie McLane on my behalf and for being someone I always wanted to be seated next to over years of passovers and thanksgivings. Charlie McLane, for going to bat so enthusiastically for some kid he'd never met. All the folks at HGL, starting with Peter Huyakorn who was immediately willing to take a chance on me. I appreciate his commitment to support me financially while at UVM through HGL, but I continue to be moved by his personal investment in my development as a scientist and a person. Jeff Fairbanks, who has always been my point-person with HGL and has been a calm and steadying presence when I did not necessarily feel either calm or steady. Glen Dewillie for always giving me straight talk, looking out for me unconditionally, and never being too busy for an email, phone call or text (even when I know he was often, in fact, too busy). Tim Hazlett, for being my intellectual kindred spirit, encouraging me to think big, and occasionally letting me know that I was not losing my mind. Larry Deschaine, for always being willing to give me a nudge in the right direction. Nikos Fytilis for, helping me navigate new academic and professional waters.

Before thanking friends and family, I would like to spend a few words thanking my undergraduate thesis advisor, Joel Franklin. Now even more than at the time, I appreciate the simultaneously irreverent (toward the institutions of science) and

serious (toward the work) attitude that he modeled for all his students. Science should be fun, and I am so grateful that my first scientific mentor made sure to remind me of that continuously.

Thanks to my friends, Devin for keeping me sane and providing a sounding board for the day-to-day issues both big and small. Laura for always knowing what to say to get me out of my head, and for being so supportive that I at times feel guilty. Ethan for maintaining his ambition and idealism despite his cynicism, and reminding me to do the same. RUT and the entire Burlington ultimate community, particularly the kids on the Burlington High School ultimate team who I have had a blast coaching. Ian McCahill for always being appropriately outraged at (insert foil here) whenever I complained or was at the end of my rope. Shaurav and Josh for not falling out of touch – I miss you guys. Linnea and Alex, for never letting me get away with a swollen head.

Finally, my family. It is obvious that none of us would be the people we are today without our families, but at this moment I am pretty happy with how I turned out and my parents and sister deserve a lions share of the credit for that. On a more practical note, my parents and my grandparents have provided me financial support without complaint or hesitation, and while I know they did so willingly and happily I believe my gratitude should not be unspoken. Especially thanks to my Grandma Betty, who couldn't quite make it to see me finish this thesis but I am sure would have been (as she always was) cheerful and refreshingly unsurprised.

Table of Contents

List of Figures

Chapter 1

Comprehensive Literature review

1.1 Bridge scour

Bridge scour is defined as the removal of stream bed soil and sediments from the supports of bridge foundations caused by water-induced erosion (Arneson et al., 2012)(Briaud et al., 2014). It is the most common cause of bridge failure in the United States (Cardoso and Bettess, 1999); of the approximately 500,000 bridges in the Department of Transportation database built over water, hundreds can be expected to experience flows of magnitude equal to or greater than the 100-year flood annually (Arneson et al., 2012).

Bridge failure and damage from scour can be both deadly and expensive. 1993 flooding in the upper Mississippi basin caused 23 bridge failures and an approximated $13 million of damage, and the cost of bridge failure can be 2-10 times the cost of the bridge itself (Arneson et al., 2012). 1994 damage to Georgia bridges was estimated to be $130 million. Analysis of damage to bridges in Vermont during tropical storm Irene found that the average cost of repair was $230,000 per bridge for the 61% of over 300 bridges affected by the storm that experienced scour damage (Anderson et al.,

2014). A study of the total economic impact of bridge failures, taking into account direct repair costs and secondary costs incurred such as increased travel time, reduced productivity, and injuries and fatalities, found that an average bridge failure has a total cost of over $13 million (Briaud et al., 2014).

The Federal Highway Administration recommends a variety of countermeasures to reduce bridge scour risk, and also provides recommended equations for estimating bridge scour under various hydrologic conditions (Arneson et al., 2012). These equations are largely empirical in nature, and depend on parameters such as the skew of the bridge, water velocity at bridge structures, and water surface elevation. Calculated scour scales positively with both water velocity and elevation. However, these equations are known to be overly conservative and relatively poor quantitative predictors of bridge scour (Sheppard et al., 2014).

To reduce the risk of bridge scour, bridge designers are encouraged to make conservative calculations of scour potential for the design flood and to provide a safety margin beyond that when planning the depth of foundations or piles (Arneson et al., 2012). Protective measures, such as rip-rap, are also recommended (Arneson et al., 2012)(Chiew, 2008). Moving away from the components of a bridge that are in the channel, research has been done to allow more accurate prediction of scour at abutments that sit in the floodplain during floods (Kouchakzadeh, 1997)(Sturm and Janjua, 1994). The relationship between channel geometry and scour depth in abutments terminating in the floodplain has also been investigated (Cardoso and Bettess, 1999).

Research that incorporates the larger hydrologic system of the river/bridge system has been, by comparison, relatively sparse. It has been shown that in some cases, the degree of constriction of the channel at and near the bridge can increase the risk of scour damage (Anderson et al., 2014). Some work has also been done

investigating the efficacy of various methods of stream restoration which considers the larger stream system in a more comprehensive way (Johnson et al., 2002). To the best of the my knowledge, no research specifically looking at the effect of floodplain access away from the bridge site on bridge scour has been published. It is reasonable to assume that it is accepted and understood by the field that flood wave attenuation via increased floodplain access will mitigate bridge scour to some degree.

Hydraulic models can be used to predict bridge scour, such as HEC-RAS (Brunner, 2016a). HEC-RAS version 4.1 is a 1-D model, but 2-D modeling can also be used in assessing bridge scour, as in (Rossell and Ting, 2013).

1.2 Optimization

The use of numerical optimization in engineering is well-established. Numerical optimization has been coupled with process-based models of varying complexity to minimize the cost of groundwater remediation designs or monitoring, design the shape of a radio antenna for satellites, and optimize the control of hydroelectric power plants, among other applications (Deschaine et al., 2013)(Hornby et al., 2011)(Li et al., 2015)(Shlomi et al., 2010). Optimization problems are varied; it can be employed in scenarios where the goal is to minimize costs subject to a set of constraints, such as finding the least-cost pump-and-treat system that reduces contaminant concentrations below a target threshold in a specified amount of time (Deschaine et al., 2013). Constraints can be enforced explicitly, using a technique such as sequential linear programming. They can also be enforced by assessing a cost to solutions that are infeasible or violate constraints, effectively forcing the optimization routine towards viable candidate solutions (Hornby et al., 2011). When there are multiple competing objectives, there will be a non-dominated front. Multi-objective optimization meth-

ods aim to return a set of non-dominated solutions. Multiple objectives can also be treated sequentially as single-objective problems, giving solutions on either extreme end of the non-dominated front (Li et al., 2015).

Alternatively, multiple objectives can be combined in a scalar function that rewards better results for both objectives (Hornby et al., 2011)(Neelin et al., 2010). This implicit or explicit weighting of two or more objectives creates a cost function with an optimum that represents a single point on the non-dominated front but may result in results that are outside of the acceptable ranges for one or more of the objectives (Neelin et al., 2010).

Sensitivity analyses have also been used in engineering applications combined with optimization (Mesfin and Shuhaimi, 2010)(Liou et al., 2013). These sensitivity analyses typically involve quantifying the sensitivity of the cost function to changes in design variables, near the optimal solution or otherwise (Liou et al., 2013). No publications were found that interpreted the optimal results themselves as relative sensitivity or as a way of prioritizing variables with respect to an objective or constraint.

Differential evolution is a heuristic evolutionary global optimization algorithm first proposed in 1997 in (Storn and Price, 1997). It is a gradient-free method, making it generalizable to problems where gradient information is unavailable, and has been succesfully used for many design optimization problems in engineering, including satellite antenna performance in (Hornby et al., 2011).

1.3 Data assimilation, parameter estimation and sediment transport

1.3.1 Data Assimilation

Data assimilation (DA) is a class of methods used for combining the prediction of a model with a noisy measurement to produce a higher-precision estimate of state variables of interest (Eppstein, 1997). The Kalman Filter (KF) produces the best linear unbiased estimator if the state transitions are linear (Eppstein, 1997)(Kim et al., 2014). The Extended Kalman Filter can be used by linearizing non-linear state transition dynamics (Eppstein, 1997)(Kim et al., 2014)(Nasab et al., 2014). Other methods for data assimilation for non-linear systems provide similar functionality, but varying performance depending on the application (Samuel et al., 2014).

These methods have been used for a variety of applications in hydrology and environmental science and engineering. Applications include improving the performance of a process-based 3-D groundwater model (Li, 2007), improving calibration performance of process-based models by augmenting the state vector being estimated (Eppstein, 1997), modeling the dynamics of lake algal blooms (Kim et al., 2014), and estimating streamflow (Nasab et al., 2014)(Samuel et al., 2014).

All of the applications I was able to find required having a calibrated model before beginning the data assimilation process. Some approaches produced high-speed model emulators as part of the DA process, e.g. (Kim et al., 2014). This is useful in situations where simulations are very computationally expensive. However, none of the works I was able to find allowed for an uncalibrated model to be used at the outset of the data assimilation process. Likewise, the calibration occurring concurrently with the data assimilation and producing a calibrated model appears to

be a novel contribution of this thesis.

The application of numerical optimization to calibration of process-based models by minimizing the disagreement of the model with respect to calibration parameters is conceptually a trivial leap from the process of manual calibration and so will not be discussed in great detail in this literature review, except to say that it is done and is particularly useful in scenarios where the model is computationally slow or has many parameters (Li, 2007)(Neelin et al., 2010).

1.3.2 Sediment Transport

Sediment transport in rivers and streams can be categorized into bed load, suspended load and dissolved load (Perillo and Lavelle, 1989). Basic modeling of sediment concentration can be a simple regression done to construct a functional relationship between flow and concentration (Hamshaw, 2014)(Perillo and Lavelle, 1989). More sophisticated data-driven approaches have used combinations of stream monitoring and meteorological data with artificial neural network algorithms to predict sediment dynamics (Hamshaw, 2014).

Process-based models of sediment transport necessarily involve many parameters due to the inherent complexity and non-linearity of the physics involved (Berenbrock and Tranmer, 2008). The sediment modeling supported by HEC-RAS, for example, employs empirical equations within the process-based modeling framework to estimate things such as the sediment capacity for a given set of hydraulic conditions or the settlement velocity of sediment particles (Brunner, 2016b). The result is that the process-based HEC-RAS modeling framework has numerous parameters that must be set.

One of these, the Critical Shield's Number, is a dimensionless parameter in the transport function used to model bed sediment mobilization and is related to

the critical shear stress (Lamb et al., 2008). It has a default value in HEC-RAS of $c = 0.039$, which is also the most common value used, but it can be defensibly set at anything between 0.029 and 0.049 (Berenbrock and Tranmer, 2008) The size distribution of the mobile bed sediment is likely to contain some non-trivial uncertainty (Olsen et al., 2005) and so also makes a good candidate for a calibration parameter.

1.4 Goals and Thesis Organization

The overall goal of this research is to develop efficient wrappers (specifically, a heuristic optimization algorithm and a Kalman filter) to leverage the advantages of process-based models and large amounts of multiple data types associated with data rich environments. Two projects to that end are presented in this thesis. The first is the construction of an optimization wrapper using Differential Evolution (DE) for performing sensitivity analysis on floodplains by ranking channel locations according to the impact that floodplain access has on bridge scour. A multi-objective cost function was constructed that minimized (1) contraction scour at a fixed bridge location and (2) the need to widen the channel floodplain. The manuscript introduces the development of a method of for providing sensitivity information for the purpose of decision support. The optimization problem is solved using DE, which is wrapped around a process-based 1-D river model (HEC-RAS) to assess the relative sensitivity of floodplain access with respect to bridge scour at different locations along the channel. This is presented as a journal article manuscript in Chapter 2. The second project wraps a data assimilation algorithm (Extended Kalman filter) around an initially uncalibrated model to create a modeling framework that dynamically recalibrates the existing model (i.e., improving prediction of state variables and associated uncertainty) as new data are acquired on a continuous basis. The method is devel-

oped with sediment transport in mind, but tested on a synthetic pendulum system. The pendulum methods and results are presented in the first half of Chapter 3 following a general introduction and motivation; the second half of the chapter shows the potential implementation of the method using a HEC-RAS sediment transport model. Overall conclusions are included in Chapter 4.

Chapter 2

Heuristic assessment of sensitivity using differential evolution: a case study for linking floodplain encroachment and bridge scour

Abstract

Background: Access to natural floodplains during extreme storm events is a key factor in mitigating the damage from flooding and erosion to structures near river corridor. This has implications for the design of many environmental and civil infrastructure problems. Bridge scour, which is the erosive removal of streambed or bank material from around bridge supports, is one of the major and expensive problems related to flood wave mitigation. However, while the constraint-free best solution is to restore access to a natural floodplain by removing built encroachments, this is rarely feasible. Costs limit remediation options, and many built structures such as roads, homes, or levees that protect valuable property are givens for the design of a remediation plan.

Results: This work leverages the benefits of process-based models by wrapping a numerical optimization technique (Differential Evolution) wrapped around a hydraulic model (HEC-RAS) to prioritize locations, both up and downstream of a bridge, with respect to their importance for reducing bridge scour during flood events. To do this, a model of the Quinan Covered Bridge in Shelburne, Vermont is used for proof-of-concept. Stream flow is artificially constricted within the channel for initial simulations. Optimization is then employed to determine the most efficient relaxation of floodplain restriction to reduce bridge scour. The optimal solution is used to assess floodplain access sensitivity at all locations along the modeled reach. Sensitivity ranking was identical across multiple weightings of stakeholder objectives, indicating that the method is robust and not overly dependent on a particular weighting of competing objectives.

Conclusion: This approach has significant potential as a decision-support tool for engineers and stakeholders responsible for designing and implementing projects where floodplain access is a concern. The methodology may be applied generally to other systems with spatially varying parameters which impact objectives or constraints to visualize the spatial variability of impacts.

Keywords: Sensitivity, optimization, bridge scour, floodplain, differential evolution

Background

Optimization and sensitivity

The use of optimization to address real-world environmental and engineering problems, and provide decision-support to stakeholders is a common strategy (Rios and Sahinidis, 2012). Optimization has been coupled with process-based models of varying complexity to minimize the cost of groundwater remediation or monitoring designs

(Deschaine et al, 2013), to design the shape of a radio antenna for satellites (Hornby et al, 2011), to optimize the control of hydroelectric power plants, and for many other applications (Shlomi et al, 2010; Bartholomew-Biggs et al, 2002; Jeongwoo and Papalambros, 2010; Mugunthan et al, 2005; Marsden et al, 2004).

These all represent design optimization problems and in cases with multiple competing objectives, there is no single optimal solution (Jeongwoo and Papalambros, 2010). Instead, there are sets of non-dominated solutions (Xu and Lu, 2011; Fowler et al, 2015). Since multiple stakeholders place varying importance on the different objectives and prioritization of constraints (Fowler et al, 2015), there are tradoffs between the objectives (Kurek and Ostfeld, 2013; Fowler et al, 2015) with, for example, increases in contaminant cleanup time being weighed against monetary cost. In such cases, the two or more objectives can be combined into a total, scalar, cost or fitness function to create a single-objective problem (Kurek and Ostfeld, 2013). The set of design variables that optimize (i.e. minimize or maximize) this function then corresponds to the optimal design solution.

Sensitivity analysis can also be performed subsequent to, or concurrently with, optimization (Harsha Choday and Roy, 2013) in engineering applications (Mesfin and Shuhaimi, 2010; Liou et al, 2013). These analyses typically quantify the sensitivity of the objective function to changes in design variables (Guerra-Gmez et al, 2013), near the optimal solution or otherwise (Liou et al, 2013), providing information about the marginal impact of changes in the design – potentially valuable information for designers and other stakeholders.

In this work, we use optimization as a tool to assess sensitivity rather than to find an optimal design. The goal is to wrap optimization around a process-based fluvial model to provide insight into the system behavior and visualize the spatial relationship between variables and competing objectives. More specifically, in cases

where an objective is comprised of or more variables that are functions of space, the proposed method ranks locations according to the sensitivity of the objective to that variable. It does so, not by assessing sensitivity near an optimal solution, but instead by interpreting "optimal" results as indicative of relative – not absolute – sensitivity. Thus, the goal is to ordinally rank locations to provide decision-support information.

Such an approach has significant advantages. It limits the need to explicitly weight competing objectives, since it does not prescribe a set of "best" designs, but indicates where, spatially or temporally, a particular variable is more or less important to a given objective. The approach suggested here may be used in the more preliminary stages of planning to provide information about system behavior and guide design criteria development.

In this work the proposed method is applied to a real hydrologic system – a 1,025 m stretch of a river and a fixed bridge location. Using floodplain access (a spatially-dependent quantity) and bridge scour (the objective), we wrap an evolutionary algorithm around a widely used process-based fluvial model to rank locations up and downstream of the bridge according to the impact of floodplain access or encroachment on predicted scour at the bridge's abutments. These rankings are relative, and may be generically applied to this kind of system to aid in the optimal placement of new bridges or to direct the efficient removal of floodplain encroachments to mitigate bridge scour risk.

Bridge scour and floodplain access

Bridge scour is the removal of streambed soil and sediments from the supports of bridge foundations caused by water-induced erosion. Scour is the most common cause of bridge failures in the United States (Arneson et al, 2012). Flooding in 1993 caused the failure of 23 bridges in the upper Mississippi basin at an approximate

cost of $13 million and in the following year, flooding was responsible for $130 million of damage to bridges in Georgia (Arneson et al, 2012). More recently, Tropical Storm Irene damaged over 300 bridges in Vermont and 61% of the affected bridges had scour-related damage (Anderson et al, 2014). The average cost of repairing the scour damage from Tropical Storm Irene has been estimated at $239,000 per affected bridge (Anderson et al, 2014). Arneson et al (2012) estimated the cost of a bridge failure to be 2-10 times the cost of the bridge itself. The available case studies have indicated that repairing a scour-damaged bridge after-the-fact is onerously expensive, and remediating scour-critical bridges *a priori* may be more economical in the long run.

The costs above include only the direct costs of repair. If a bridge must be closed for repairs or fails altogether, there are cascading secondary costs due to lost time and decreased productivity of travelers, not to mention the very real risk of injuries and fatalities if scour damage results in unexpected and sudden bridge failure. When these secondary costs are considered, the total average cost of a single bridge failure is estimated at $13 million (Briaud et al, 2014) – and over 23,000 bridges were classified as scour critical in 2011 in the United States, representing nearly 5% of all bridges (Arneson et al, 2012). Given that scour is the leading cause of bridge failure and that hundreds of bridges are expected to experience flooding in excess of the 100-year flood annually (Arneson et al, 2012), the scale of this infrastructure management problem is clear.

Floodplain constriction is a key factor in scour damage risk (Anderson et al, 2014) as floodplains are vital to the attenuation of flood waves during storm events (Luke et al, 2015). Thus from the perspective of bridge scour, increases in channel flow, velocity and water surface elevation can lead to increased scour potential. Mitigating scour risk by restoring floodplain access away from the bridge would help

attenuate flood waves and result in smaller peak stage and discharge during storm events, which has obvious benefits that extend beyond bridge scour mitigation. However, floodplain encroachments often comprise infrastructure such as homes, businesses, and roads that local stakeholders are reluctant to remove or even alter. In addition, some interventions are more expensive than others, and countermeasures may be more or less cost-prohibitive at different locations up and downstream of an existing bridge.

The importance of floodplain constriction by bridge structures is fairly well understood and various works have investigated these effects or calculated bridge scour at abutments in the floodplain (Kouchakzadeh, 1997). However, to the best of our knowledge, prior research investigating the impacts of floodplain constriction (other than bridge structure constriction) on scour has not been published. A tool that can assess the relative sensitivity of bridge scour to floodplain access at different locations in a river reach has obvious benefits for this scenario.

In addition to mitigating scour at existing bridges, consideration of floodplain access is important when planning the location of new bridges. An understanding of the relative sensitivity of floodplain access at different locations has the potential to be very powerful. As previously mentioned, a bridge itself constitutes floodplain encroachment and becomes essentially part of the hydraulic and hydrologic river system. Whether the engineering problem at hand is to mitigate risk for a bridge at a fixed location, or optimal placement of a new bridge to minimize scour risk within design constraints, or best placing an unavoidable encroachment when flexibility exists, understanding the sensitivity of scour to floodplain access at different locations both up and downstream of the bridge (existing or proposed) is key.

Differential Evolution

Differential Evolution (DE) is a stochastic, population-based evolutionary algorithm (Rios and Sahinidis, 2012) designed for global optimization of real-valued functions with multiple variables (Storn and Price, 1997). These design variables specify a design solution that is evaluated by combining one or more objectives into a scalar valued objective function. This function can then be optimized. It is often referred to as a cost function when the design problem is framed as a minimization problem or a fitness function when framed for maximization in the context of evolutionary algorithms. For this work, minimization was chosen and the function to be optimized will be referred to throughout as the cost function. Generally, constraints can be treated either as additional objectives to be minimized with penalty terms added to force convergence to feasible solutions (Bartholomew-Biggs et al, 2002). They can also be enforced explicitly with the search constrained to feasible regions of the search space (Storn and Price, 1997).

DE is an evolutionary algorithm, which solves real parameter and real value problems (Storn and Price, 1997). The process of DE starts with initialization of the population, selected from a uniform distribution that covers the entire parameter space. Individual candidate solutions are modified using biologically-analogous mutation and crossover operations to explore the search space. These operations are controlled by two parameters, the crossover fraction and the mutation factor. Details on the mechanisms of the algorithm are described by Storn and Price (1997). DE has been shown to outperform many other evolutionary algorithms on standard benchmark and real-world problems (Vesterstrom and Thomsen, 2004).

DE has been successfully used on a cost function containing an implicit weighting of multiple objectives, resulting in a significantly improved design (Hornby et al, 2011). These kinds of tradeoffs encoded in a cost or fitness function have been dis-

cussed and utilized in applications including satellite antenna design (Hornby et al, 2011), optimizing the performance and operation of hydroelectric power plants (Li et al, 2015), and optimal management of groundwater remediation and management (Rizzo and Dougherty, 1996; Deschaine et al, 2013). Sensitivity of the cost function to changes in the design variables near the optimum (Dougherty and Marryott, 1991) is one way to evaluate relative sensitivity. However, interpretation of the optimal values of the decision variables themselves as relative sensitivity has not been proposed to the best of our knowledge.

Methods

Study site and site model

The selected study area is the Lewis Creek channel and adjacent floodplain in vicinity of the historic Quinlan Covered Bridge in Charlotte, northwestern Vermont (Figure 2.1). The study reach is 1,025 m long. The upstream drainage area of the river at this location is approximately 180 square kilometers. The Quinlan Bridge span (Figure 2.2) is less than the natural bankfull width of the Lewis Creek channel, and the bridge is oriented at a sharp angle to the Lewis Creek. Flows are constricted through the bridge span leading to upstream aggradation and scour of the bridge abutments. Roads in vicinity of the bridge are elevated above the flood plain and both laterally and vertically constrain the channel and floodplain on approach to the bridge. Ice jams regularly cause localized flooding upstream and downstream of the bridge, threaten the integrity of the abutments of this historic bridge, and subject a nearby residential property to inundation and fluvial erosion hazards (South Mountain Research and Consulting and Milone & MacBroom, Inc., 2010). In 2010, an analysis of the bridge was contracted to provide recommendations on several alternatives to

Figure 2.1: Counter-clockwise from top-right: the location of the study site within Vermont; an aerial view of the modeled reach; and a picture of the bridge from the downstream side.

existing conditions for the purpose of reducing the risk of further damage. Mitigation scenarios considered included lowering adjacent roads, lowering the floodplain, removing berms and realigning the bridge (South Mountain Research and Consulting and Milone & MacBroom, Inc., 2010). To perform the analysis, a HEC-RAS model was built, calibrated and validated. HEC-RAS (Hydrologic Engineering Center-River Analysis System) is a widely used river and stream modeling software (Goodell, 2014) designed and distributed by the U.S. Army Corps of Engineers (USACE.) It supports modeling of many hydraulic structures, including bridges, and simulations of alternatives provide the predicted physical variables needed (such as velocity and stage) to

evaluate scour and erosive potential for proposed scenarios. To evaluate and compare multiple scenarios related to encroachment HEC-RAS was used as a proof of concept.

(a) (b)

Figure 2.2: The view of the bridge from upstream during a high-flow event (a) and cracking and undermining of the abutment of the bridge due to scour (b).

The reach modeled by Milone and Macbroom, Inc. is 1025 m long and drops approximately 5.8 m in elevation through the reach (Figure 2.3). The model extends from just upstream of the Scott Pond Dam (which operates in a run-of-river mode) to just downstream of the bridge, and is comprised of 13 cross sections. The model geometry shows the cross sections in plan view (Figure 2.3a) well as the a cross section of the river along its length (Figure 2.3b).

Eight cross sections out of 13 cross sections include floodplain access modifications for the proof-of-concept presented in this work. (Figure 2.1 and 2.3a) with XS1 representing the most upstream cross section and XS 8 the most downstream. The bridge is between XS 6 and XS 7.

Flow magnitudes for various return periods were calculated by Milone and MacBroom using USGS streamflow gaging data from Station #04282780 on the Lewis Creek (USGS, 2010) and regression equations (Olson, 2002). The analysis of alter-

natives was primarily done using steady-state simulations, but a sediment transport analysis was performed to investigate the potential impact of erosion and sedimentation for the proposed alternatives. The latter requires a quasi-unsteady analysis in HEC-RAS in which a transient event is modeled using a series of steady flows.

For steady flow simulations in HEC-RAS, stage and flow are calculated using energy losses between user-defined cross sections. For transient simulations, it solves the full 1-D St. Venant equations; HEC-RAS version 4.1, used for the Quinlan model, provides support only for 1-D modeling. The recently released version 5.0 provides support for 2-D flow modeling. In this work, transient simulations were used with an upstream hydrograph as a boundary condition. The hydrograph was constructed by scaling the quasi-unsteady hydrograph built by Milone and MacBroom for the sediment transport model so that peak flow corresponded with the design (50-year) flow. HEC-RAS routes this flow through the reach and provides hydraulic variables at the bridge for a given scenario.

Scour prediction

Models such as HEC-RAS provide the means to predict physical variables, such as flow, stage or velocity. These variables, in turn, can be used in empirical scour equations as described by the Federal Highway Administration (FWHA) in HEC-18 (Arneson et al, 2012).

Scour predictions were calculated in post-processing using the results of HEC-RAS simulations. The contraction scour equation is one of many outlined by the FWHA in HEC-18 (Arneson et al, 2012) and is the selected for this work:

$$Y_s = 4Y_0 \left(\frac{V_0}{\sqrt{gY_0}} \right)^{\frac{1}{3}} (0.55) K_1 K_2, \tag{2.1}$$

where:

Y_s is the scour depth [m],

Y_0 is the water elevation at the bridge [m],

V_0 is the flow velocity [m/s],

g gravitational acceleration [m/s^2], and

K_1 and K_2 are the skew and abutment coefficients, respectively.

The scour equations tend to be overly conservative (Sheppard et al, 2014). However, for the purposes of evaluating bridge scour relative to a number of proposed scenarios, referred to here as *relative scour risk*, it is safe to interpret higher contraction scour values as corresponding to increased scour risk. While our results used the contraction scour equation it is important to note that the methodology and the subsequent interpretation of the results would not change if a different scour equation was selected. As these equations are empirical, their validity is constrained to the range of data used to derive them.

When combined with the HEC-RAS model developed by Milone and MacBroom, equation (2.1) provides the needed hydraulic parameters, and enables scenarios to be evaluated and compared on the basis of bridge scour risk.

Differential Evolution (DE) optimization and HEC-RAS modifications

This design challenge can be formulated as a multi-objective optimization problem. To demonstrate the application of a method for evaluating the location-dependent sensitivity of bridge scour to floodplain access and constriction, the Quinlan HEC-RAS model geometry was modified. The modified geometry represents this stretch of Lewis Creek as having the maximum amount of floodplain access possible. The

design flood was initially (and artificially) constricted entirely to the channel, thus providing no floodplain access up or downstream of the bridge. This is a noteworthy departure from current standard engineering methods and research, as the modified model does not reflect any proposed or hypothetical scenario. Numerical optimization using DE was then used to find the most efficient removal of encroachments to minimize bridge scour at the Quinlan Bridge. To efficiently mitigate scour risk, different magnitudes of encroachment removal, i.e. floodplain access, will be needed depending on the location; scour sensitivity to floodplain access can be inferred from these optimal encroachment removal values and locations ranked by their impact on scour. Locations that require more extensive encroachment removal to reduce scour are more salient.

Once the modifications to the HEC-RAS model were implemented, a DE optimization algorithm was wrapped around the model to impose floodplain constriction, enable HEC-RAS simulations, and the post-process contraction scour results without using the graphical interface. Python code was written to provide this functionality using the HEC-RAS API (Application Program Interface (Goodell, 2014)) and the ability to read and write to the HEC-RAS text files. Removal of encroachments on both the left and right side of the channel (facing downstream) was defined along eight cross sections for a total of 16 variables. These variables are defined over a range from 0 to 1, with 0 indicating no floodplain access (full constriction) and 1 indicating full floodplain access (no constriction.) This is shown graphically in Figure 2.4, with $\vec{x}$ being a vector whose components represent floodplain access corresponding to the left or right side of a particular cross section.

Cost Function

Construction of the cost function is key, particularly when multiple objectives are involved or when constraints are being enforced using penalty terms, to ensure that solutions meet the constraints and specifications of the real-world problem. A cost function was constructed to combine and weight the two competing objectives (floodplain access and bridge scour) into a scalar value as follows:

$$f(floodplain\ access, scour) = floodplain\ access_{sum}^2 + (scour - scour_{min})^2. \quad (2.2)$$

An optimal solution is one with low floodplain access (i.e. few built encroachments) and reduced bridge scour. These objectives are inversely correlated, so the trade-offs between them are defined by a set of pareto optimal (non-dominated) solutions. The cost function weights and combines these objectives into a scalar function to be minimized. Written with more succinct notation, equation (2.2) becomes:

$$f(Y_s, \vec{x}) = \left(\sum_i \vec{x}_i \right)^2 + (Y_s - Y_{s\_min})^2 \quad (2.3)$$

The cost function is equal to the sum of the squares of the floodplain access parameters ($\vec{x}_i$, where i indexes location) and the amount of bridge scour (Y_s) over baseline scour (Y_{s_min}) as determined by a simulation with fully open floodplains. It is a function of the entire set of floodplain access parameters encoded in $\vec{x}$ and the scour, which is an implicit function of $\vec{x}$, since the level of scour depends on the hydraulic behavior given a specified floodplain access scenario.

If the goal were to peform design optimization and identify a single floodplain design that maximizes encroachment along the eight selected channel locations while

minimizing scour at the bridge, rather than evaluate sensitivity of individual locations along the channel, weighting parameters could be added to each term in equation 2.3 to define the trade-offs between the two stakeholder objectives. For the purposes of performing a sensitivity analysis, weights that determine the relative importance of objectives are not necessary because the optimal values of floodplain access will be evaluated relative to one another. In other words, they will be used to rank locations according to sensitivity and their absolute values will not be considered. To test this assumption, equation (2.3) was modified with a weighting factor, β, as follows:

$$f(Y_s, \vec{x}) = \left(\sum_i \vec{x}_i \right)^2 + \beta (Y_s - Y_{s\_min})^2. \tag{2.4}$$

Larger values of β implicitly place greater weight on scour reduction, while values closer to zero weight maximization of floodplain access more heavily. Optimization was performed using values of β that relatively weight the two objectives over two orders of magnitude.

In this work, the DE implementation in the Python library, SciPy, based on the description given by Storn and Price (1997), was wrapped around the combined HEC0RAS cost function framework. The crossover fraction was set to 0.7 and the mutation factor sampled from a uniform distribution in $(0.5, 1)$ every generation. The population size was 10. Because DE is a stochastic method, optimization was repeated using random restarts to verify consistent convergence. For each of the three values of the weighting parameter β from equation (2.4), batch runs of 10 random restarts were performed.

Results

Flood wave mitigation

An initial exploratory investigation of system behavior was performed to guide future testing. The scour gradient was calculated using a one-sided finite difference and defined as the rate of change of scour with respect to changes in floodplain access (Figure 2.6). All sixteen components of the gradient are shown in terms of the physical locations they represent. Labels "XS 1" and "L" and "R" refer to the left and right overbanks, respectively, of cross section one. The figure shows the approximate partial derivative of scour with respect to the corresponding component of $\vec{x}$. Figure 2.6 identifies only XS 7, the location immediately downstream of the bridge, as having any noteworthy effect on bridge scour; all other locations have a negligible impact on simulated bridge scour.

To complement this finding, the up and downstream hydrographs for the 50-year design storm for a simulation reflecting maximum floodplain access were plotted to assess the extent of flood wave attenuation and the role of naturally available floodplain access in the system. These hydrographs are shown in Figure 2.5. There is no discernible difference between the up and downstream hydrographs, and therefore, no flood wave attenuation. This simulation reflects the maximum amount of floodplain access, so no other plausible scenario would result in increased flood wave attenuation. The most likely explanation for this result is that the reach is simply not long enough and does not have sufficient storage volume in the floodplains. If upstream floodplain access does not attenuate flood waves, then bridge scour for the design flood will be controlled by backwaters created by downstream constriction. When viewed together, the scour gradient and hydrograph data provide convincing justification for focusing only on the variables corresponding to cross section 7 given

the trivial impact that other locations have on bridge scour

Global search results

The optimal results generated by applying DE to three cost functions representing different weightings of objectives ($\beta = 0.1$, $\beta = 1$ and $\beta = 10$) are shown in Figure 2.7 in coordinates normalized by the size of the floodplain. For the purpose of sensitivity analysis, the ranking of two variables (i.e. the amount of left and right floodplain access at cross section 7) should be roughly independent of weighting; all solutions should be on the same side of the line defined by $y = x$. Optimal solutions below and to the right of the 45° line correspond to solutions where $XS_7^L > XS_7^R$. Solutions above and to the left of this line correspond to solutions where $XS_7^R > XS_7^L$. Optimal solutions for all three cost functions fall on the same side of the $y = x$ line and indicate the same sensitivity ranking of variables.

The results of all 10 batch runs for all 3 cost functions are shown together in Figure 2.7 to confirm consistent convergence of DE. DE is a stochastic algorithm, so to increase confidence in the optimal results produced by DE random restarts were performed on all three cost functions. There is no way to ensure that the location it converges to is a true global optimum; thus random restarts (with different pseudo random number generator seeds) that converge to the same optimal solution increase the chances of finding a globally optimal solution or provide evidence that the initial results are not local sub-optimal solutions. For each cost function, the results are clustered in the same region of the search space indicating that convergence was consistent and representative of globally optimal solutions.

Discussion

The methodology implemented in the prior sections provides a framework for decision support in the form of a sensitivity analysis. Using optimization and a process-based model, the proposed methodology assesses the spatial variability of the impact of one objective on a system constraint. The system in this case is a river channel and the constraint of interest is contraction scour at a fixed bridge location. For demonstration purposes, optimization was performed using DE to minimize a cost function that increases with increasing bridge scour (the constraint) and increasing floodplain access (the spatially-dependent design variable.) The desired outcome is a sensitivity analysis that ranks floodplain access by location in terms of impact on bridge scour under a defined design flow (i.e., flood of 50-yr return interval).

Optimization performed on this system results in a set of spatially dependent optimal floodplain access values. The proposed method is distinct from the design optimization process, instead leveraging numerical optimization and a cost function to evaluate the relative spatial sensitivity of one objective with respect to another. Although it is straightforward to rank locations according to their respective optimal values, the interpretation of this information as relative sensitivity is not. The optimization process performed in this work provides evidence that this is a reasonable interpretation. The scour gradient at maximum constriction can be easily interpreted as relative sensitivity by noting that locations where the scour is reduced more per unit of increased floodplain access have a greater impact on bridge scour.

These results suggest that bridge scour at the Quinlan Bridge system is controlled primarily by a backwater created by downstream constrictions. This implies that upstream reach storage effects at this particular site do not significantly mitigate the design flood wave. The up and downstream hydrographs at maximum floodplain

accessibility confirmed this interpretation, showing very little flood wave mitigation between the top and bottom of the reach (Figure 2.5). The gradient results (Figure 2.6) also indicate that only the cross section immediately downstream of the bridge had any noteworthy effect on bridge scour, and that scour was more sensitive to floodplain access on one side of that cross section than the other. The finding that only downstream floodplain constriction causing backwater has an impact on bridge scour is specific to floodplain access and is a result of insufficient upstream storage area in the floodplains. The channel is vertically disconnected from much of the study reach at the stage of the 2-year flood – significantly lower than the 50-year design storm used for performing the sensitivity analysis. This may partially explain the lack of floodplain storage (and resultant neglibible flood wave attenuation).

Optimization of the cost function was consistent for all three cost functions (values of weighting parameter β) with identical rankings of the two salient decision variables. Optimization resulting in identical ranking of variables for all three values of β indicates that the sensitivity analysis is roughly independent of the weighting of the objective terms in the cost function. A result of this finding is that the method does not rely on a precise weighting of objectives by stakeholders – the sensitivity analysis is identical across objective weights. While the site in question does not have upstream sensitivity, in a reach with more salient locations (i.e. more locations where floodplain access impacts bridge scour) the method could be applied analgously to rank more than the two locations ranked in this work.

The reliability of the underlying model itself is important when assessing the reliability of the sensitivity analysis. In this work, energy losses and erosive effect, due to sharp changes in direction of the stream channel, cannot be modeled using the 1-D St. Venant equations solved in HEC-RAS 4.1. In their report, Milone and MacBroom noted the sharp turn in the stream immediately preceding the bridge.

One of the bridge scour mitigation measures briefly considered was to realign the stream and straighten its approach to the bridge. However, from a stream geomorphic perspective it was judged to be both prohibitively expensive and ultimately ineffective.

However, this sharp turn in the stream channel is something to be considered in terms of its impact on the sensitivity results. A picture of the sharp approach is shown in Figure 2.2a. Without a more detailed representation of the site physics (e.g. a 2-D model), it is difficult to determine the extent to which the 1-D HEC-RAS modeling approach oversimplifies the bridge scour and erosion dynamics. Two dimensional modeling, like that now available in HEC-RAS 5.0, would be a logical next step to confirm the sensitivity findings of this work, and to evaluate the site itself as a candidate for further study using 2-D models. However, even without this 2-D analysis there are good reasons to trust the results. Thus, the conclusion implied by the sensitivity analysis that downstream floodplain access is more salient to bridge scour mitigation than access upstream is a direct result of this finding, and it is therefore likely that substituting a 2-D model would not substantively change the sensitivity analysis. Even if there are noteworthy erosive effects not captured in the 1-D model, these would be more relevant to accurate and quantitative prediction of bridge scour at the site than the sensitivity analysis presented in this work.

Conclusions

This work presents a new approach to applying DE optimization to engineering challenges, and tests that approach on a real site. The technique involves constructing a cost function in such a way that the multi-objective "optimal' results do not represent an optimal design in the traditional sense of minimizing a collective set of two or more constraints, but rather represent the sensitivity of a given constraint or objective of

interest with respect to a second objective or constraint – a novel interpretation of optimization results. Because optimal decision variable values are assessed relative to one another and do not represent a specific design or reflect stakeholder-defined preferences of objectives, the need to specify the relative importance of objectives is relaxed. The constraint used to demonstrate the approach was bridge scour with respect to floodplain access, and the system was a river system comprising natural channel geometry and built structures (a bridge). The use of differential evolution on cost functions representing different weightings of the two objectives provided the same rank-order of reach locations with respect to their floodplain access impact on bridge scour; ancillary testing using a finite difference scour gradient supports the proposed interpretation. Also of interest is that the sensitivity analysis is somewhat independent of objective weighting, which potentially reduces the stakeholder burden of deciding how to weight competing objectives. Instead, this approach focuses analysis the system's behavior that can be used to guide the design of floodplain infrastructure, remediation efforts, or the placement of new bridges. Applying this approach to other rivers would focus attention on locations where increased floodplain access would result in the most efficient use of resources, and applying it to other systems with spatially-variable components which have functional relationships with objectives of interest to stakeholders could provide similar decision-support information.

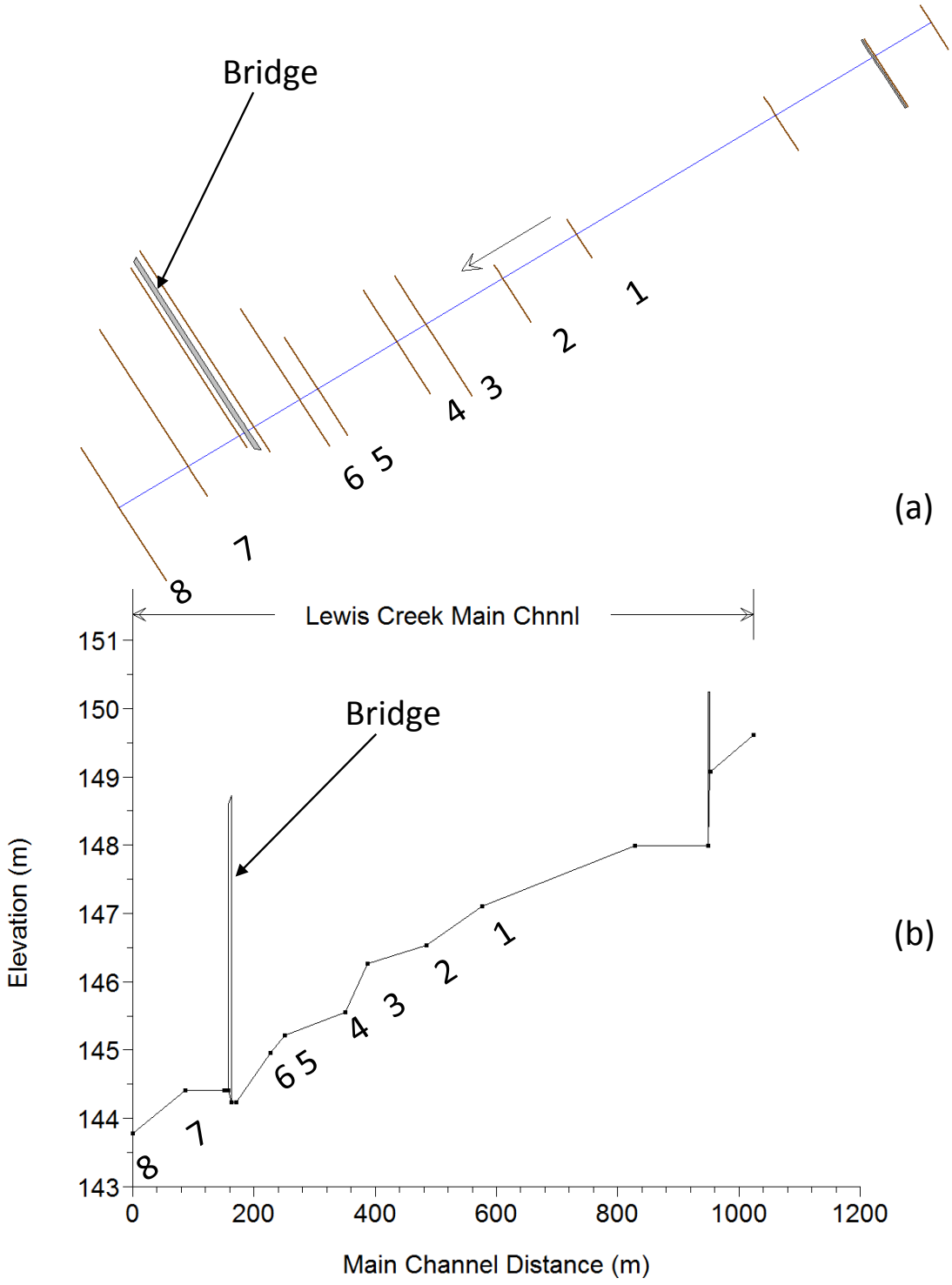

Figure 2.3: The model geometry of the Quinlan bridge is shown with its 13 cross sections (a). The direction of flow is from the upper-right to the lower-left. In (b), a side view of the modeled reach is shown. The Mill Pond dam can be seen at right and the bridge at left.

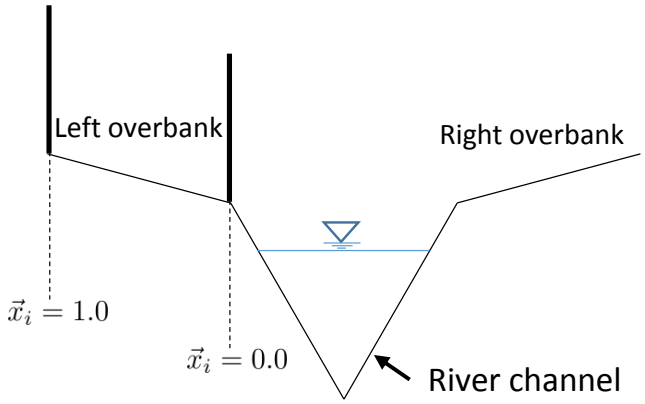

Figure 2.4: Schematic showing removal of floodplain constrictions. For the location corresponding to the i^{th} component of the decision vector, $\vec{x}_i = 0$ specifies no relaxation of the constriction, i.e. no flow is permitted to access the floodplain. $\vec{x}_i = 1$ specifies full floodplain access, ie. no encroachments.

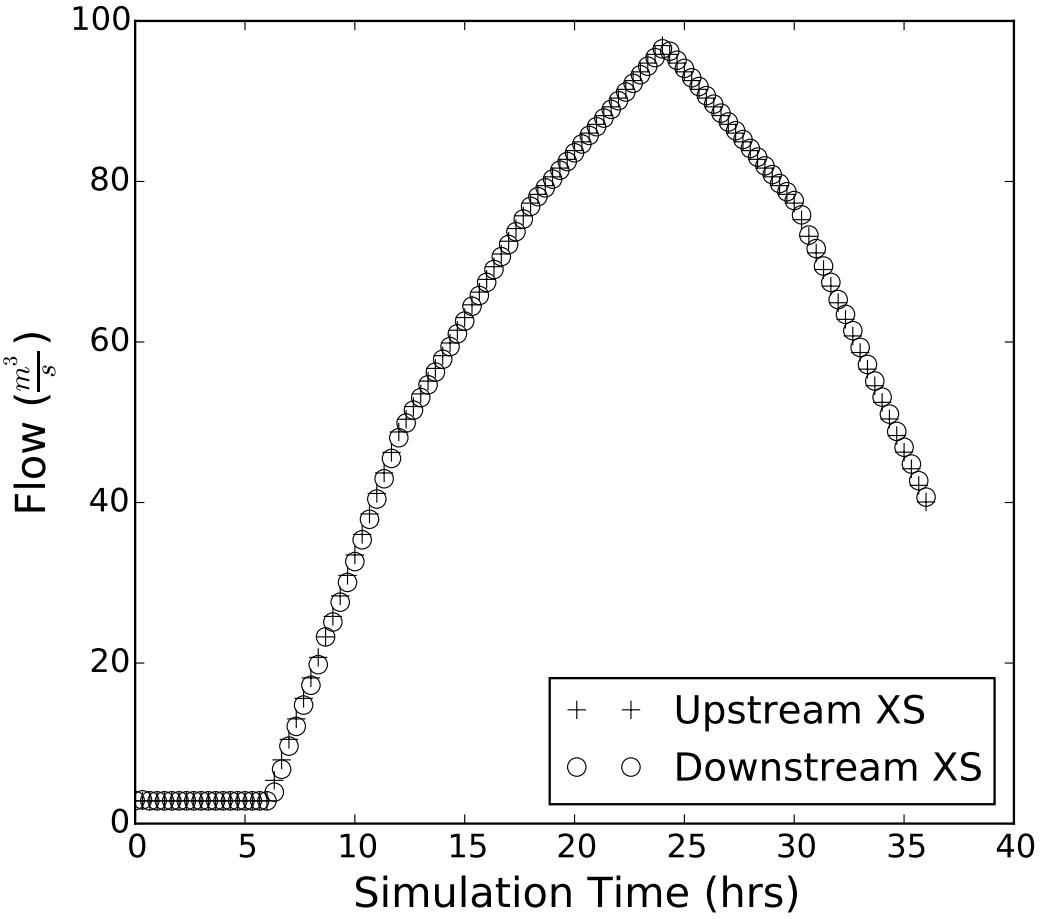

Figure 2.5: Hydrographs at the most upstream and most downstream channel cross sections for a simulation performed with no floodplain constriction.

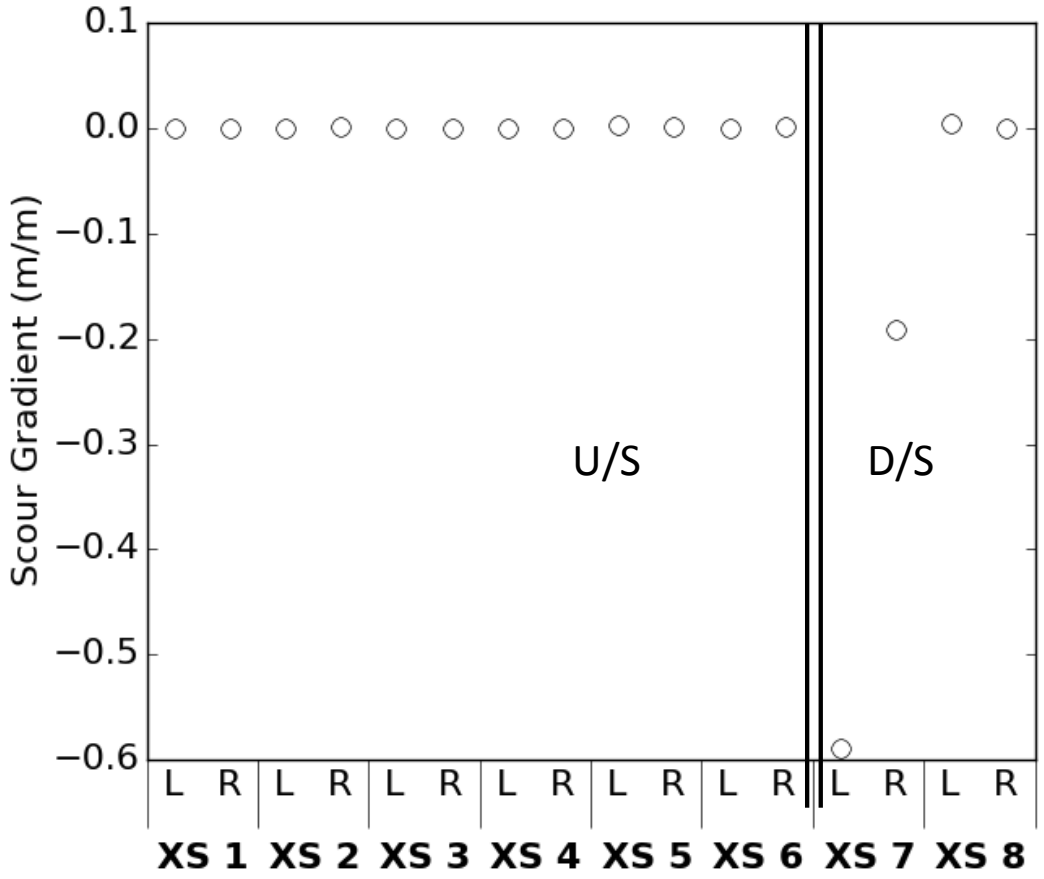

Figure 2.6: The scour gradient, measured in meters of scour reduction per meter of encroachment removal, is shown for both the left and right overbanks for each of eight cross sections. The most upstream cross section (XS 1) is at the far left and the most downstream (XS 8) at the far right.

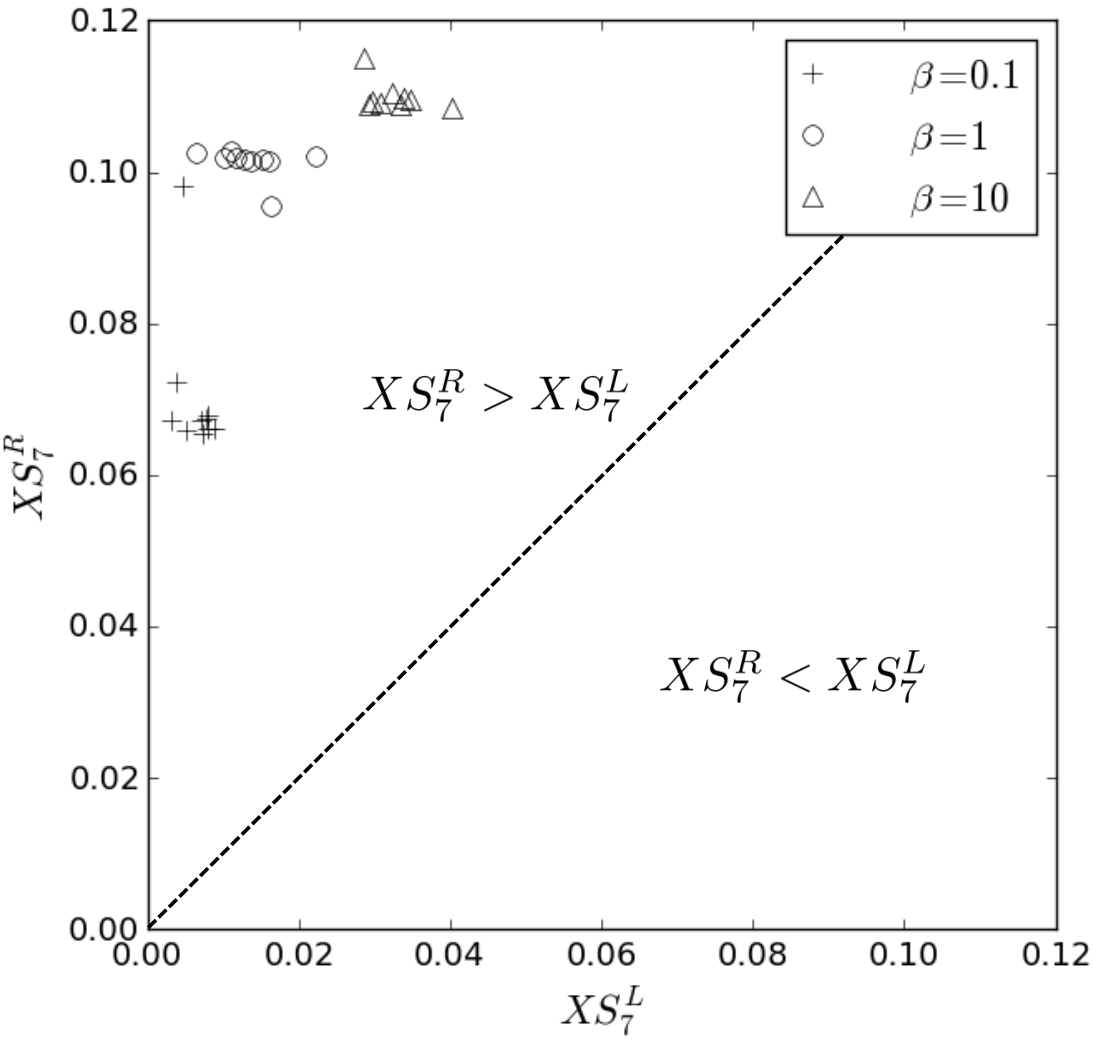

Figure 2.7: Initial optimization results in the original decision-variable coordinates for all 3 weightings of the two objectives

References

Anderson IA, Dewoolkar MM, Rizzo DM, Huston DR (2014) Scour related vermont bridge damage from tropical storm irene. In: Structures Congresss, pp 505–515

Arneson L, Zevenbergen L, Lagasse P, Clopper P (2012) Evaluating scour at bridges. Tech. rep., National Highway Institute

Bartholomew-Biggs M, Parkhurst S, Wilson S (2002) Using direct to solve an aircraft routing problem. Computational Optimization and Applications 21:311–323

Briaud JL, Gardoni P, Yao C (2014) Statistical, risk, and reliability analysis of bridge scour. Journal of Geotechnical and Geoenvironmental Engineering 2(140)

Deschaine LM, Lillys TP, Pinter JD (2013) Groundwater remediation design using physics-based flow, transport and optimizatioin technologies. Environmental Systems Research 2(6)

Dougherty DE, Marryott RA (1991) Optimal groundwater management: 1. simulated annealing. Water Resources Research 27(10):2493–2508

Fowler K, Jenkins E, Ostrove C, Chrispell J, Farthing M, Parno M (2015) A decision making framework with modflow-fmp2 via optimization: Determining trade-offs in crop selection. Environmental Modelling & Software 69:280 – 291

Goodell C (2014) Breaking the HEC-RAS Code: A User's Guide to Automating HEC-RAS. h2ls

Guerra-Gmez I, Tlelo-Cuautle E, de la Fraga LG (2013) Richardson extrapolation-based sensitivity analysis in the multi-objective optimization of analog circuits. Applied Mathematics and Computation 222:167 – 176

Harsha Choday S, Roy K (2013) Sensitivity analysis and optimization of thin-film thermoelectric coolers. Journal of Applied Physics 113(21):214906

Hornby GS, Lohn JD, Linden DS (2011) Computer-automated evolution of an x-band antenna for nasa's space technology 5 mission. Evolutionary Computation 19(1):1–23

Jeongwoo H, Papalambros PY (2010) Optimal design of hybrid electric fuel cell vehicles under ununcertain and enterprise conditions. Journal of Fuel Cell Science and Tecnology 7(2):021,020–021,020–9

Kouchakzadeh R S an dTownsend (1997) Maximum scour depth at bridge abutments terminating in the floodplain zone. Canadian Journal of Civil Engineering 24(1):996–1006

Kurek W, Ostfeld A (2013) Multi-objective optimization of water quality, pumps operation, and storage sizing of water distribution systems. Journal of Environmental Management 115:189 – 197

Li FF, Schoemaker CA, Qiu J, Wei JH (2015) Hierarchical multi-reservoir optimization modmodel for real-world complexity with application to the three gorges system. Environmental Modeling and Software 69:319–329

Liou CD, Wang KH, Liou MW (2013) Genetic algorithm to the machine repair problem with two removable servers operating under the triadic (0, q, n, m) policy. Applied Mathematical Modelling 37(1819):8419 – 8430

Luke A, Kaplan B, Neal J, Lant J, Sanders B, Bates P, Alsdorf D (2015) Hydraulic modeling of the 2011 new madrid floodway activation: a case study on floodway activation controls. Natural Hazards 77(3):1863–1887, DOI 10.1007/s11069-015-1680-3

Marsden AL, Wang M, Dnnis Jr JE, Moin P (2004) Optimal aeroacoustic shape design using the surrogate management framework. Optimization and Engineering 5:235–262

Mesfin G, Shuhaimi M (2010) A chance constrained approach for a gas processing plant with uncertain feed conditions. Computers & Chemical Engineering 34(8):1256 – 1267

Mugunthan P, Shoemaker CA, Regis RG (2005) Comparison of function approximation, heuristic, and derivative-based methods for automatic calibration of computationally expensive groundwater bioremediation models. Water Resources Research 41(11):n/a–n/a, w11427

Olson SA (2002) Flow-frequency characteristics of vermont streams. Water-Resources investigations report 02-4238, USGS

Rios LM, Sahinidis NV (2012) Derivative-free optimization: a review of algorithms and comparison of software implementations. Journal of Global Optimization 56(3):1247–1293

Rizzo DM, Dougherty DE (1996) Design optimization for multiple management period groundwater remediation. Water Resources Research 30(2):483–197

Sheppard D, Melville B, Demir H (2014) Evaluation of existing equations for local scour at bridge piers. Journal of Hydraulic Engineering 140(1):14–23

Shlomi S, Ostfeld A, Rubin H, Shoemaker C (2010) Optimal groundwater contamination monitoring using pumping wells. Water Science and Technology 62(3):556–569

South Mountain Research and Consulting, Milone & MacBroom, Inc (2010) Quinlan bridge area alternatives analysis to reduce flood and erosion risks. Tech. rep., Lewis Creek Association

Storn R, Price K (1997) Differential evolution – a simple and efficient heuristic for global optimization over continuous spaces. Journal of Global Optimization 11:341–359

USGS (2010) National water information system. Web interface

Vesterstrom J, Thomsen R (2004) A comparative study of differential evolution, particle swarm optimization, and evolutionary algorithms on numerical benchmark problems. In: Evolutionary Computation, 2004. CEC2004. Congress on, vol 2, pp 1980–1987 Vol.2

Xu Z, Lu S (2011) Multi-objective optimization of sensor array using genetic algorithm. Sensors and Actuators B: Chemical 160(1):278 – 286

Chapter 3

A Hybrid Data-Assimilation and Parameter Estimation Method

3.1 Background and Motivation

Modeling of physical phenomena to support engineering and public policy decision making, or to improve understanding of the underlying system(s), generally falls into one of several categories depending on the amount and quality of data available and the level of detail at which the underlying processes are understood. In situations where data are sparse but there is good understanding of the underlying process dynamics, physics-based models (or process-based models) may be used. These models are built by generating approximate solutions to the governing equations, whether derived from first principles or empirical equations. On the other hand, for problems that have an abundance of data but llack a complete description of the dynamics, data-driven models are used. These can range in complexity from straightforward linear regression to sophisticated multi-layer artificial neural network or machine learning algorithms, but ultimately they all depend on a plethora of prior

data and information to make predictions (McDonnell et al., 2007).

In practice, the dichotomy described above is not absolute. There are almost always some data and understanding of the underlying processes. Increasingly, as remote sensing technology and data storage capacity increase, the amount of data available for almost any engineering problem will be significant (Szalay and Gray, 2006). Where the dichotomy breaks down is in the kind of data available. It is easy to imagine scenarios where stakeholders want information about watershed dynamics. In the case of hydrologic surface water and sediment modeling, the issue is likely not a lack of data – the USGS has many gauging sites throughout the country, and meteorological data is plentiful. The issue is that the available data, while related to the information the stakeholders want or need, is not that information. Furthermore, much of this secondary data is available at multiple, often irregular, temporal and spatial, making inference of the dynamics of actual interest even more challenging (McDonnell et al., 2007).

In this ambiguous space between a data-rich and data-poor environment, a physics-based model will often appear to be more trouble than it is worth. These models typically have significant sensitivity to physical parameters that are more difficult and resource intensive to collect than typically collected by sensors. For example, in surface water modeling, these parameters might be roughness coefficients. In groundwater models, it is typically the hydraulic conductivity field. These parameters must be adjusted to match observed behavior during calibration; a model that is not calibrated is of little use for making quantitative forecasts. If data for model calibration and validation are unavailable, moving to a purely data-driven model may be warranted.

However, a calibrated physics-based model can be an incredibly powerful tool. Unlike data-driven models, physics-based models can be applied to scenarios that

are outside the strict range of data on which the model was calibrated. If system behavior in previously sparsely observed regimes is of interest, a data-driven model has limited utility, while a well calibrated physics-based model will often provide good predictions in this type of situation. Physics-based models can also produce estimates and predictions of variables for which *no* measurements are available – provided it has been successfully calibrated to other variables. Unfortunately, even when traditional calibration data are available in sufficient quantity, model calibration is a tedious (often manual) process of adjusting parameters and performing simulations. Even when automated parameter estimation is used, models of some systems (e.g. climate prediction) can be challenging to calibrate due to the complexity and number of parameters and quantity of data (Neelin et al., 2010).

In this work we describe a system for integrating non-traditional and disparate data sources with process-based modeling to create a robust modeling framework. The Extended Kalman Filter is used to dynamically recalibrate a process-based model to the data-assimilated state estimate at specified time steps. In principle, data could be fed into the system in real-time.

3.2 Methods

3.2.1 The Kalman Filter

Kalman filters are widely used tools in signal processing and other fields where the interpretation of noisy, time series data is necessary. If the system is linear, meaning that the transition from one time step to the next can be represented as a linear operation, then the Kalman filter produces an optimal estimate of the signal by combining the noisy measurement and model prediction. The filter is optimal in the sense that it minimizes the expectation value of the mean-squared error of its

estimate.

Formally, assume that the state of the system at time step i is represented by a vector $x_i \in \mathbb{R}^m$. The transition to the next time step is governed by:

$$x_{i+1} = Ax_i + Bu_i \tag{3.1}$$

with $u \in \mathbb{R}^n$ a vector of external control inputs that is known *a priori* and may generically be a function of time. A and B are square weight matrices that encode the linear dynamics of the state transitions.

There are also direct measurements of the state at each time step $z_i \in \mathbb{R}^m$ that have some associated random noise, which is assumed to be normally-distributed, unbiased and stationary. There is also process noise associated with the linear state transition, so in actuality the transition dynamics are:

$$x_{i+1} = Ax_i + Bu_i + w \tag{3.2}$$

and

$$Hx_{i+1} = z_{i+1} + v, \tag{3.3}$$

where z is the measurement of the state vector at time step $i+1$, and $w \in \mathbb{R}^m$ and $v \in \mathbb{R}^m$ are the measurement and process noise represented by independent random variables. For simplicity, the random variables will not be subscripted because they have static probability density functions, but at each time step the density function is newly sampled and so the random noise at time step $i+1$ is not equal to the noise at time step i.

The filtering problem, with these definitions, can be described in the following way. Given two estimates of the state vector x at time step $i+1$, one given by a noisy measurement, z_{i+1}, and another by the estimate of the state at the previous

time step, x_i, find weight(s) K – the Kalman gain – such that

$$\hat{x}_{i+1} = K_{i+1} z_{i+1} + (1 - K_{i+1})\hat{x}_i, \tag{3.4}$$

results in the minimum of the squared estimate error

$$\sum_{j=1}^{m} (\hat{x}_{i+1}^{j} - x_{i+1}^{j})^2 \tag{3.5}$$

with $\hat{x_i^j}$ representing the best estimate of the j^{th} parameter of x at the i^{th} time step.

The above formulation can be modified for more complex systems and applications, e.g. the measurement does not have to have the same dimension as the state vector. In such a case there is an additional linear operator that maps a state vector to a measurement vector. In a simple example, if the state vector is

$$\vec{x} = \begin{pmatrix} x \\ \\ \dot{x} \end{pmatrix}, \tag{3.6}$$

the position and velocity of a particle, but only the position is measured, then the measurement operator will be

$$H = \begin{pmatrix} 1 & 0 \end{pmatrix}. \tag{3.7}$$

Applying this operator to $\vec{x}$ maps the position and velocity vector to the position.

3.2.2 The Extended Kalman Filter

The Kalman Filter is limited by its application to systems where the state transitions are linear. To get circumvent this, if the state transitions are non-linear functions

the transitions can be linearized around the current state using Taylor expansion. The state transition matrices are replaced by the Jacobians of the non-linear transition functions. This is known as the Extended Kalman Filter, and it is the data assimilation algorithm that will be employed here.

3.2.3 Case study I: simple pendulum

For the purpose of testing the combined EKF/dynamic calibration method, a synthetic system was selected. The system chosen is the simple pendulum, governed by

$$\frac{d^2\theta}{dt^2} = -\frac{g}{L}\sin(\theta), \tag{3.8}$$

where,

θ is the angle of the pendulum [radians]

g is the gravitational acceleration [meters/second^2]

L is the length of the pendulum [meters]

This system has several properties that allow many of the key EKF elements to be explored. It is non-linear, allowing for complex dynamics in certain regimes. There is no general closed-form solution, and it is simple enough that accurate numerical solutions can be generated relatively easily. It has dependence on the pendulum length, L, which may be used as a calibration parameter, and its non-linearity creates sensitivity to changes in L, as well as the initial conditions.

To generate synthetic data, Verlet integration was used to solve equation 3.8. This method is symmetric about the current time step and is time reversible, resulting in approximate conservation of energy for generated solutions (Franklin, 2013). To represent the "true" system state, Verlet was applied with $\Delta t = 0.001$ s for $t \in [0, 10]$,

with $L = 1$, $\theta_0 = 0.5$ and $\dot{\theta}_0 = 0$. The "model" is represented by a Verlet-generated solution with time step $\Delta t = 0.1$ s. The state vector to be estimated by the EKF is the angle of the pendulum, θ, and the angular velocity, $\dot{\theta}$:

$$\vec{x}_k = \begin{pmatrix} \theta \\ \dot{\theta} \end{pmatrix} \tag{3.9}$$

with k indicating that the state represents the k^{th} time step in the filtering process. $\dot{\theta}$ is an output of the model, calculated using a one-sided finite difference, although it could be explicitly modeled by transforming equation 3.8 into vector form.

Measurements to be used for assimilation with model prediction were produced by adding normally distributed random noise with standard deviation 0.05 to the earlier-generated true state angle at 0.1 second increments.

The EKF as applied to the pendulum proceeds as follows:

For $i = 1, 2...10$

1. The Verlet model runs and predicts the angle and angular velocity at $t + 0.1$ seconds.

2. The noisy synthetic measurement of the angle at $t + 0.1$ seconds is assimilated with the model prediction using EKF.

3. The initial conditions (angle and angular velocity) are reset in the model to correspond to the filtered state estimate.

Steps 1-3 are repeated for all time steps until $t = 10$.

Initially, to replicate what the process would be for a real application, the EKF is wrapped around the model assuming perfect calibration (i.e. initial conditions and pendulum length are set exactly the values used for generating the data). Next, to be more realistic, the model was calibrated using a local optimizer (L-BFGS-B) to

minimize the squared prediction error and the EKF process was repeated with this calibrated model. The length and initial angle were used as calibration parameters. In both instances, the EKF was re-run with different process and measurement error covariance matrices to improve performance.

To test the EKF method, incorrect values for pendulum length and initial angle were used at $t = 0$: $L = 1.1$ and $\theta_0 = 0.4$. At every time step, the model is run from $t = 0$ to produce a predicted state vector. After assimilation, several approaches were used for calibration, with all techniques calibrating to the EKF state estimate rather than the measurement. The first approach calibrated the model only to the current state. The second approach calibrated the model at every time step to a moving window of past state estimates. The final method calibrated to the current and all previous state estimates. In all instances, the best estimate for both the initial angle and pendulum length were tracked throughout the assimilation process.

3.3 Results and Discussion

3.3.1 Pendulum case study: model with perfect information

When the Extended Kalman Filter was wrapped around a model with a perfect-information (i.e., the synthetic pendulum system) it performed as expected and reduced the standard deviation of the prediction errors compared to the measurement and model errors by 19% and 42%, respectively (Figure 3.1). The top panel compares the true state, the EKF state estimates, and the measurements. The bottom panel compares the true state, the predictions using only the model (run from $t = 0$ to $t = 10$ with perfect information) and the EKF state estimates.

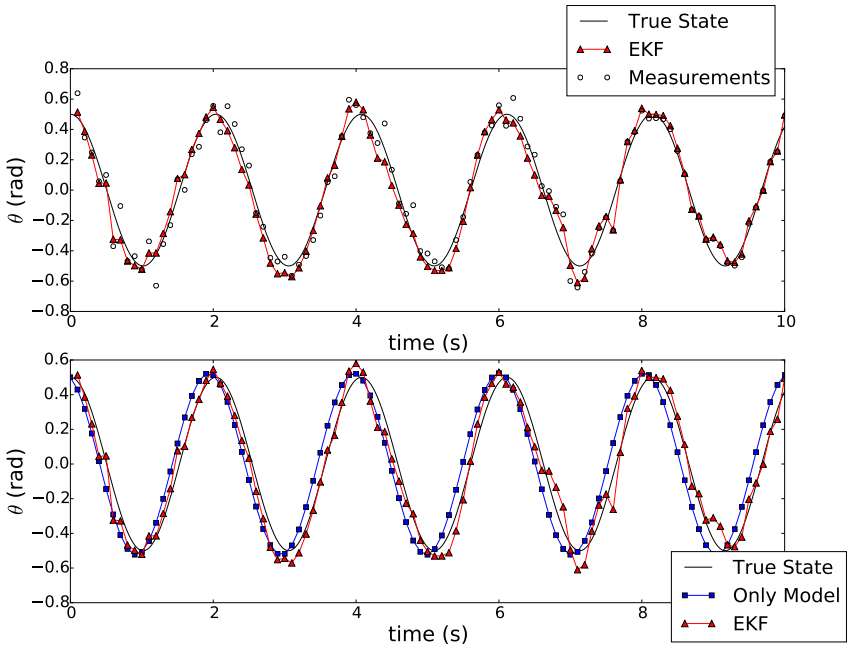

Figure 3.1: EKF results using a perfect-information model (i.e., synthetic pendulum system), compared to the true state and (a) the measurements and (b) the stand-alone model.

3.3.2 Pendulum case study: model calibrated to noisy measurements

When the model was calibrated to the noisy measurements rather than using the exact parameters to generate the data, the calibration parameters were found to be $\theta_0 = 0.4885$ and $L = 1.0398$. The true values are 0.5 and 1, respectively. The EKF results from using the pre-calibrated model again show that the algorithm performs as expected (Figure 3.2).

It is worth noting the comparison of the perfectly informed model (Figure **??**b) with the model-only performance in the perfect-information test (Figure 3.1a). In the first test, the numerical results slightly underestimates the period, causing drift compared to the true state. In the second, the calibration parameters result in the opposite effect – a slight overestimate of the period. However, both simulations

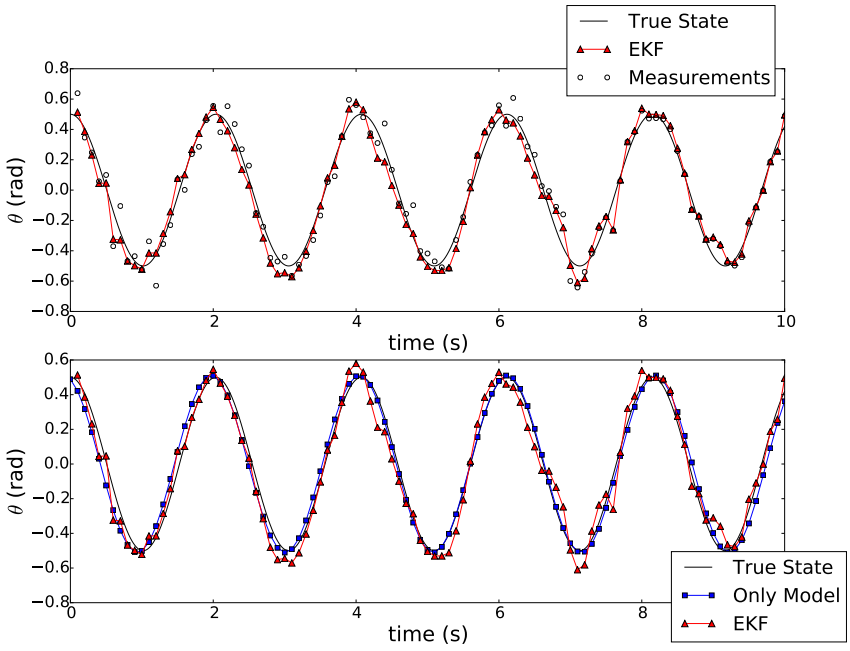

Figure 3.2: Results of using the EKF with a pre-calibrated model, compared to the true state and (a) the measurements and (b) the stand-alone model at bottom.

show modeled peaks preceding the true peaks at the beginning of the simulation and occurring later than the true peaks toward the end of the simulation. The calibration came very close to adjusting the parameters to better match their true stael values. This is important because it means that a traditionally calibrated model will have a fudge-factor built into its calibration that is specific to the originally calibrated data, and will not be flexible to new data, except through the addition of that data into its calibration set.

3.3.3 Pendulum case study: dynamic recalibration

The test in which the model was recalibrated to only the current filtered state at each time step resulted in unstable estimates of calibration parameters over time. This makes some intuitive sense, given that only information from a single measurement is being assimilated into the parameter estimates. The results of this EKF

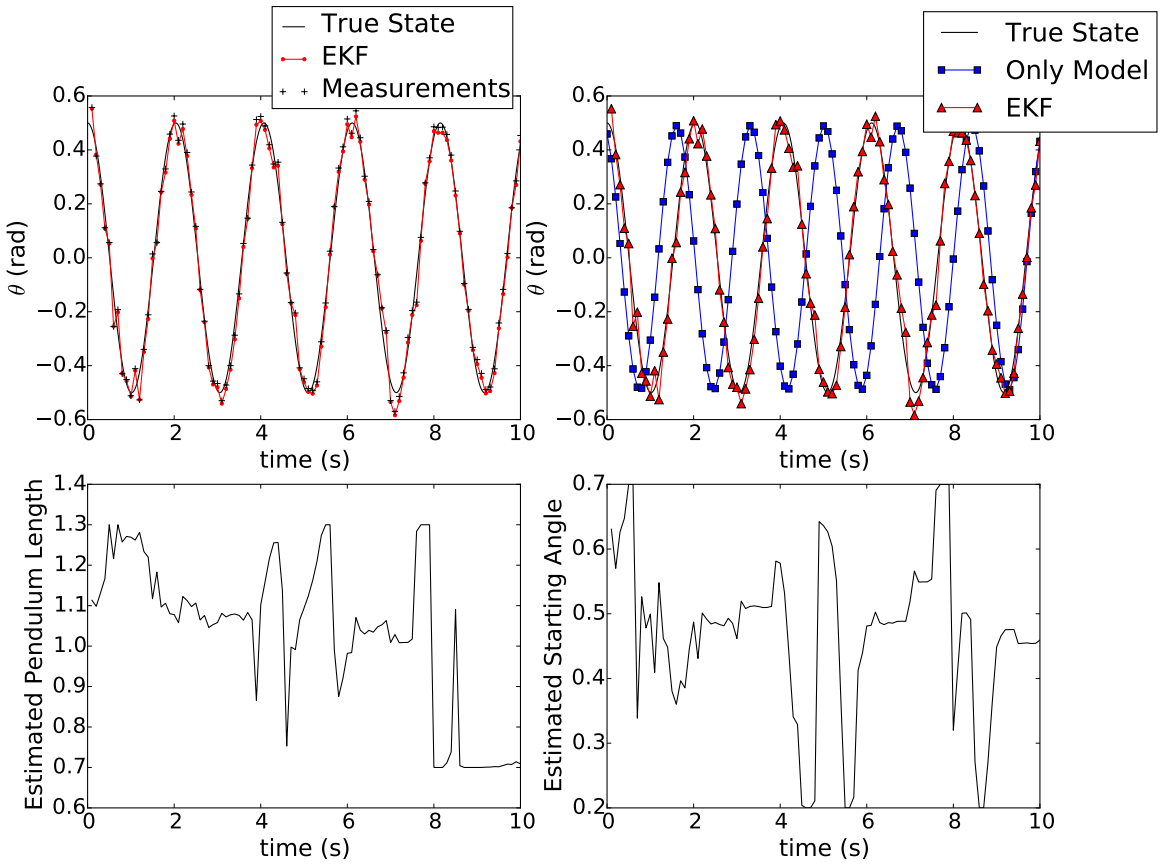

Figure 3.3: Results of using EKF with a dynamically recalibrated model performance compared to the (a) measurements and (b) stand-alone model. The bottom two graphs show the trace of the calibration parameters over time.

implementation are shown in Figure 3.3.

The EKF states qualitatively appear to agree with the true states and measurements in a manner similar to the EKF from sections 3.3.1 or 3.3.2. However, when the model is re-run from time zero using the most recent estimate of the calibration parameters, it becomes clear that the model has not been successfully calibrated. Instead, because of the periodicity of the system, there are multiple sets of initial conditions and pendulum length that result in a predicted angle at a specific time that is close to the true angle – even though the error at all other times is very high. This causes the instability in the calibration parameter estimates over time.

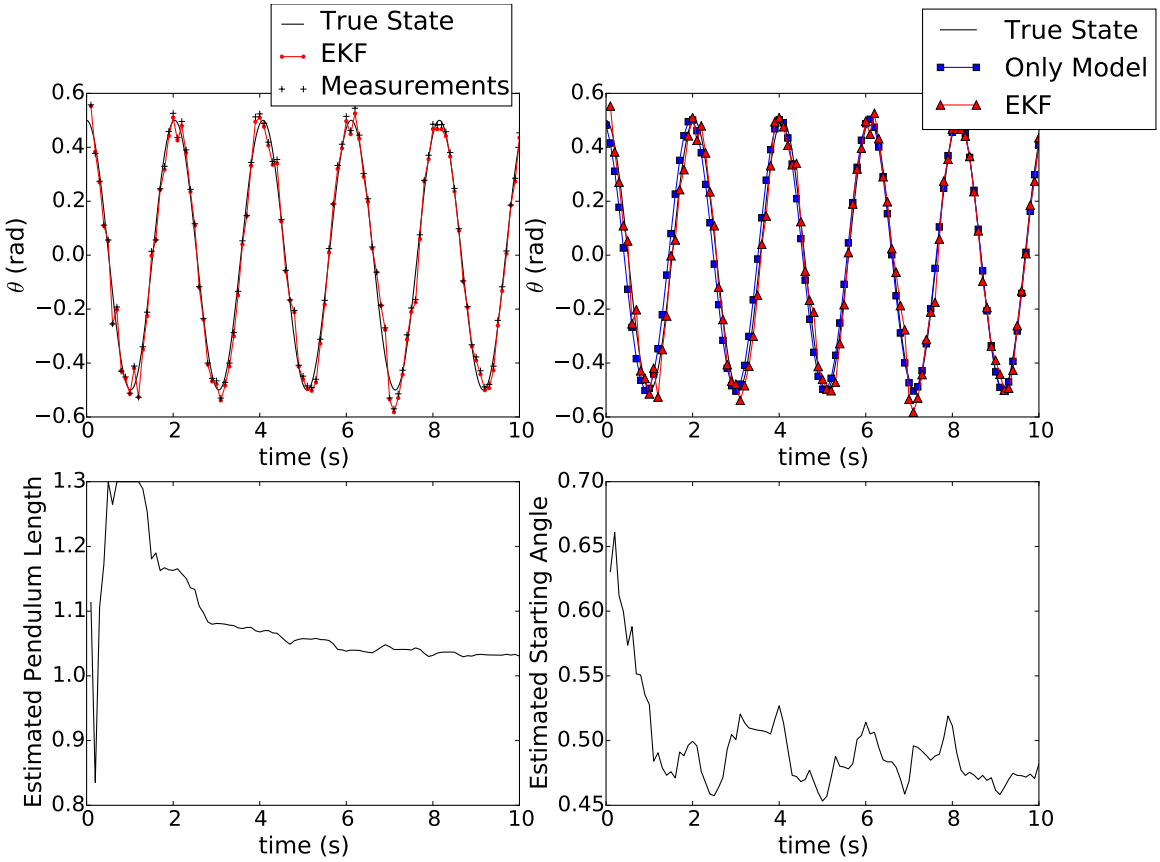

Figure 3.4: The EKF best estimated calibration parameters using a moving-window of 10 time steps (1 second) for dynamic recalibration.

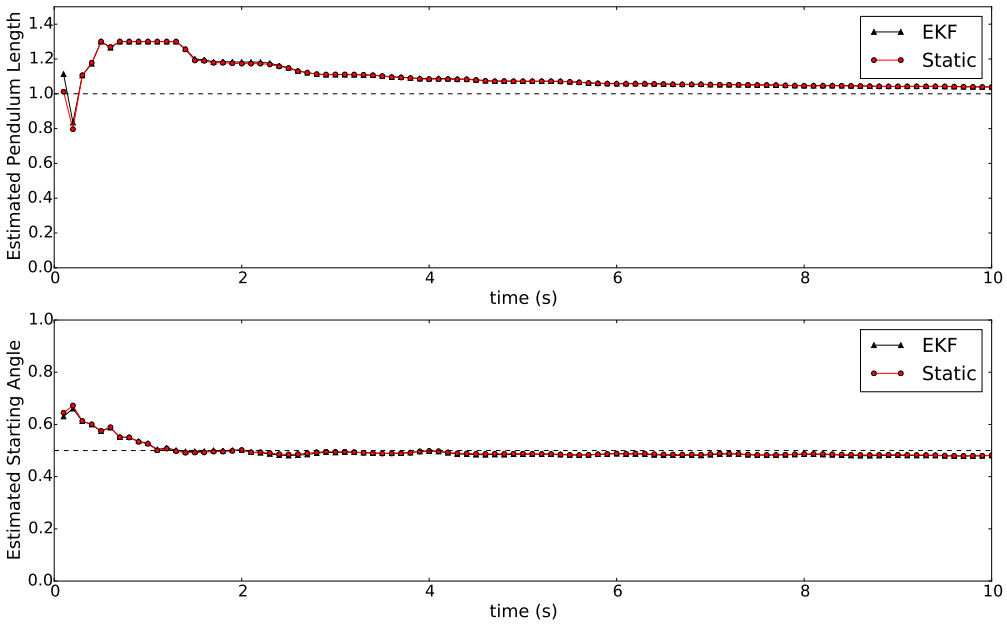

Figure 3.5: The EKF best estimated calibration parameters are shown over time, alongside the originally (static) calibrated parameter values with all measurements up to that time step.

Calibration to the current and all previous states or to a moving window of past states should help address this problem, making the parameters more biased to prior parameter estimates at nearer time steps. Using a moving window of past state estimates to calibrate the model produced much better parameter estimates (Figure 3.4). There is no evidence of the stability issues present in 3.3, with both parameter traces converging. The oscillations in the estimate for θ_0 represents some fundamental uncertainty in estimates of model parameters, and this approach makes that uncertainty more apparent and explicit than static calibration would.

Figure 3.5 demonstrates one of the benefits of this approach. It includes the parameter traces for the dynamic calibration with a comparison to traditional calibration, i.e. minimizing measurement error. At every time step, the values of the calibration parameters using all previous measurements are shown. Both calibration

methods have similar convergence properties, and converge to the correct values of parameters. However, until sufficient calibration data for model validation exist, the model cannot be used to make forecasts. The traditional calibration doesn't converge until $\approx t = 5$ s and cannot be used until after this time. In contrast, the EKF system makes predictions with higher precision than measurements alone from time zero, before the calibration parameters converge.

Conceptually porting these observations to real-world problems and models, it is plausible to propose a situation where a system experiences an event outside the regime of previous observations. With a model pre-calibrated to past observations, the model might not be calibrated for this new regime. If the new regime persists, the model will have to be recalibrated from scratch. The EKF system, in contrast, continues making state predictions and will simply adjust its estimate of the calibration parameters to reflect the new regime, automatically leverage new data on a continuous, potentially real-time, basis to keep the model calibrated. If the sediment transport model discussed in the next section is used as an example, this scenario might be a storm or flood event larger than those used for calibration, or a change in land-use policies that alters the dynamics of the sediment system.

3.4 Sediment Transport

The modeling software used for the proposed demonstration of these concepts is HEC-RAS, a surface water model developed and distributed by the United States Army Corps of Engineers. It is widely accepted and used in both the public and private sector, and supports hydraulic modeling of structures such as dams, weirs, levees and bridges, as well as floodplain mapping and sediment transport modeling.

To demonstrate the application of the combined EKF and dynamic recalibra-

tion framework, there is no better candidate than the phenomena of sediment transport. Current physics-based models depend heavily on empirical equations and are highly sensitive to physical variables for which there is often significant uncertainty. As a result, while a calibrated model is still a powerful tool, successful calibration can prove challenging and the dynamics that are explicitly accounted for may not be inclusive enough, either with respect to producing accurate predictions or with respect to the problem of interest (or both). Simultaneously, direct measurement is difficult and often lacks precision. Even instantaneous suspended sediment samples may not provide a good snapshot, since suspended sediment concentration often varies significantly with depth. Samples are some combination of time and/or depth integrated. Direct measurement of channel geometry change due to erosion or deposition can be more precise with the right tools, but obtaining these kinds of measurements regularly is prohibitive.

Despite these challenges, the sediment and watershed modeling environment is becoming more data-rich. Terrestrial LIDAR provides highly precise monitoring of stream banks; aerial drones are starting to do the provide similar data, but more cheaply and over wider areas. High temporal resolution turbidity data are sometimes used as a proxy for suspended sediment concentration. Combining the information content in these data streams with the information built into physics based sediment transport models has the potential to radically change how these systems are analyzed and improve the accuracy and usefulness of the modeling tools.

The reach selected for testing this new dynamic calibration and assimilation framework has a significant amount of high time-resolution data. Turbidity sensors are used to estimate suspended sediment concentration at both the top and bottom of the reach taking measurements at 15 minute or less time intervals. There are also pressure transducers measuring stage at these locations, and an additional pressure

transducer in the middle of the reach. In addition, time integrated suspended sediment samplers, instantaneous high-flow sediment sampling capabilities, and enough flow measurements to create at least one rating curve are all available. Surveys were performed to get stream bed geometry. Additionally, while the following data were not used for the test case, terrestrial LIDAR and digital elevation data collected via a drone as well as meteorological measurements are available for this site and could conceivably be integrated into future extensions.

What is available to us is a significant volume and variety of data at different temporal and spatial scales, but no obvious way to integrate it all into a coherent, robust model. A method for integrating this data with the process-based sediment modeling capabilities of HEC-RAS is described below – it should be noted, however, that the specific choice of model does not limit the applicability of the concept.

For transient simulations, HEC-RAS solves the full 1-D St. Venant equations. In addition the the geometry data (cross sections, reach lengths, etc.) required for steady-state simulations, transient simulations require an upstream flow or stage hdyrograph as a boundary condition. The computational time step and output intervals can be adjusted as needed for model stability and accuracy or post-processing.

The modeled reach is of the Shepard Brook, a tributary of the Mad River in the Winooski River Watershed, which ultimately drains into Lake Champlain. The reach to be modeled has a pressure transducer and turbidity sensor at both the bottom and top of the reach. At the bottom, there are sufficient discharge and stage measurements to produce a flow rating curve. The turbidity readings can be used to estimate sediment concentration (Total Suspended Solids, or TSS) with high precision as the two are highly correlated in this watershed (Hamshaw, 2014). The TSS and stage measurements at the top of the reach will be used as a boundary condition for the transient HEC-RAS model.

In addition to the hydraulic parameters necessary to build the unsteady HEC-RAS model, the grain size distribution of the suspended sediment at the top of the reach is needed as a boundary condition, as is the size distribution of the mobile streambed. Using suspended sediment samplers that take time-integrated samples as well as instantaneous samples during high flow events, a relationship between grain-size distribution and flow will be inferred. To measure the distribution of the streambed sediment, pebble counts were performed at each cross section in the model(Olsen et al., 2005).

From previous unpublished research, there already existed a nine cross section HEC-RAS model surrounding the bridge at the bottom of the proposed reach. Nine additional cross sections were surveyed upstream of the bridge creating a model $2,180$ feet long with approximately a 24 foot drop in elevation over that distance. A satellite image of the site and the new surveyed cross sections is shown in Figure **??**.

Turbidity sensors collect data at high (15 minute) temporal resolution at the top and bottom of the modeled reach. This reach was chosen such that deposition and/or erosion are likely to exist within the reach, so TSS should change between the top and bottom sensor. The HEC-RAS model would also predict sediment concentration, stage and discharge at the bottom of the reach, which can be compared to measured values.

The combined EKF and dynamic calibration framework, when applied to HEC-RAS sediment modeling, proceeds as follows. At every time step, given measured TSS, flow and water temperature at the the reach inlet:

1. Run the HEC-RAS simulation forward until the time of the next downstream TSS measurement

2. Estimate the linearized state transition matrices for use in the EKF based on

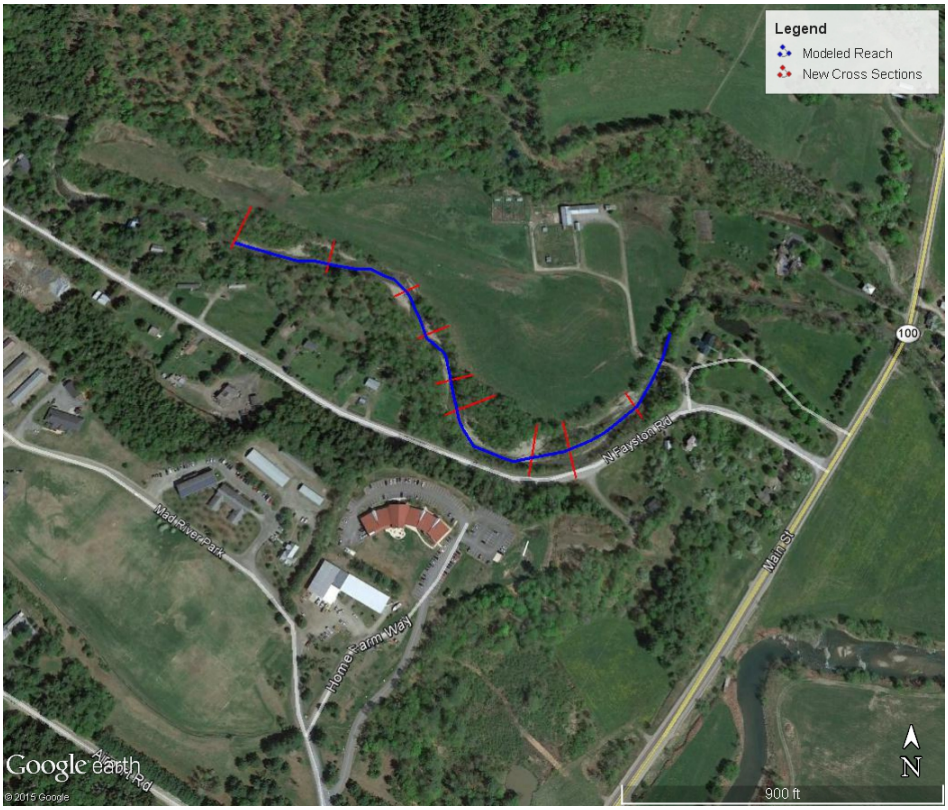

Figure 3.6: Aerial view of the proposed modeled reach with the new surveyed cross sections upstream of the bridge in red. Flow goes from left to right, with the bridge at the bottom of the reach.

this prediction

3. Calculate the Kalman Gain, and

4. Use the measured TSS and the estimate at the last time step, update the best estimate of TSS at the bottom of the reach

5. Use a local minimization method, recalibrate the HEC-RAS model calibration parameters

A visual representation of the algorithm is shown in Figure 3.7, where:
$\vec{v}_{boundary}$ is a vector of boundary condition values
$\vec{v}_{calibration}$ is a vector of calibration parameters
$\vec{x}_p$ is the predicted state vector
$\vec{x}_{i+1}$ is the estimated state vector at time $i+1$
$\vec{z}_{i+1}$ is the measurement at time $i+1$
f is a the model prediction error as a function of calibration parameters, and
ϵ is the calibration tolerance.

On the left side, calibration data and boundary condition data are fed into the HEC-RAS model which is run to the next time step. The predicted sediment concentration is assimilated with the measurement through the EKF to produce a best estimate of sediment concentration at time step $i+1$. On the right side, an optimization method find the calibration vector which decreases the prediction error below the specified tolerance, at which point the new calibration parameters are passed back to the HEC-RAS model. New boundary condition data is provided, the model runs forward another time step, and the process repeats.

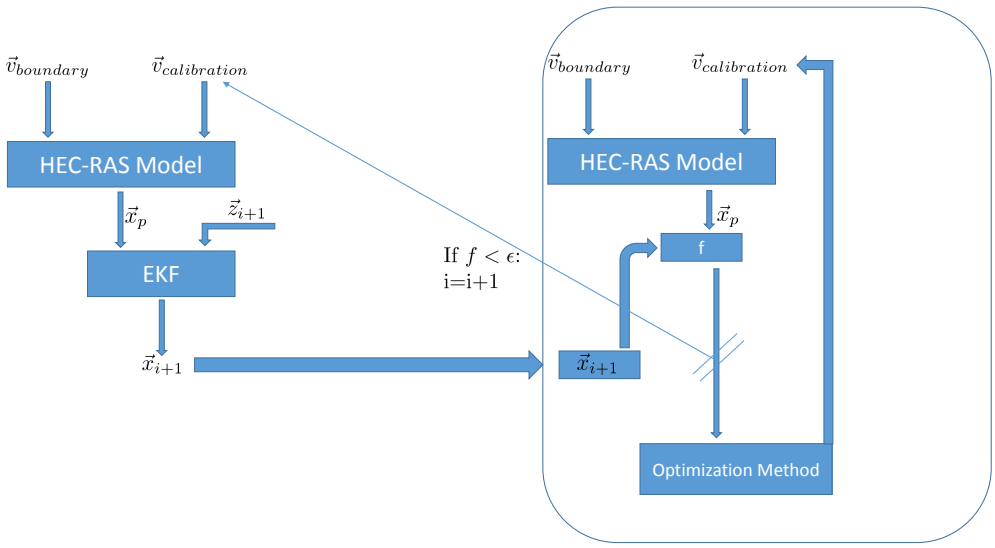

Figure 3.7: Visual representation of the combined data-assimilation and parameter estimation algorithm for sediment transport modeling in a flow chart.

3.4.1 Calibration Process

The recommended method of calibrating HEC-RAS sediment transport models involves comparing predicted channel erosion and/or deposition to measured values over periods of time of sufficient length to allow significant channel geometry change Brunner (2016). Calibrating to high temporal resolution suspended sediment concentration data, even for a relatively small model that runs quickly, would get computationally expensive very quickly. Over a month, which is roughly minimal the time scale over which we might expect significant channel geometry changes in this reach, the model output at nearly 3000 times would need to be compared to measured values. The dynamic recalibration proposed in the EKF approach addresses this challenge. Each recalibration is only to a single data point – the best estimate of TSS at the current time step. The calibration parameters are adjusted at each time step to match this best estimate. The model is then run to the time of the next measurement, the EKF produces another best estimate, and the model parameters are again recalibrated to

a single piece of data.

The downside of this approach is that the model has to be rerun from time zero during each iteration. The estimated state vector using the EKF is distinct from the initial conditions of the RAS model itself, so the only way to get an update a set of initial conditions at time step $i+1$ is to run the model from time steps 0 to i. However, given the computational speed of HEC-RAS, this is not a limiting factor. The proposed potential calibration parameters for the system and model described above are the upstream suspended sediment size distribution and the Shields number, which is related to the critical shear stress of the mobile streambed sediment. If this HEC-RAS sediment model is to be successfully integrated with the dynamic calibration/EKF framework, a method of automating the calibration at each time step is needed.

The mode calibration process can be formally described as an optimization problem. If f is a function that represents the observation error and takes a vector of the calibration parameters $\vec{x}$ as an argument, the goal of calibration is to find $\vec{x}$ such that f is minimized. The method used initially is Newton-Rhapson, a gradient descent method where the gradient will be approximated by a finite difference. If the current best estimate of the optimum at time t is $\vec{x}_c$, the next estimate will be:

$$\vec{x}_n = \vec{x}_c - \alpha \frac{f(\vec{x}_n)}{|\nabla f(\vec{x}_n)|} \tag{3.10}$$

where α is a constant between 0 and 1, and when it is set to 1, $\vec{x}_n$ is the location of the nearest zero of f assuming f is linear. Equation 3.10 is applied iteratively until $|f|$ is less than a specified tolerance. For non-linear functions where x_c is not set close enough to the minimizing vector $\vec{x}_{opt}$, this method can be prone to overshooting and non-convergence, in which case the step size α can be reduced.

If only the Shield's Number is used, then $\vec{x}$ is a scalar and the algorithm can be easily executed in one dimension with a simple upper and lower bound, determined by reasonable physical limits, as a constraint. Extending the calibration parameters to include a grain size distribution of either the incoming sediment or the streambed complicates the process. The size distribution is defined by the percentage of sediment, by weight, that is contained in various size bins – e.g. 15% between 2 mm and 4 mm. If there are N size bins, the distribution may be defined as a vector $\vec{s}$ where s_i, the i^{th} component of $\vec{s}$, is the percentage of sediment contained in the i^{th} bin. These must add up to 100%, giving a constraint equation of:

$$\sum_{i=1}^{N} s_i = 100. \tag{3.11}$$

Thus, the set of feasible size distribution vectors may be represented as a hyperplane S in $\mathbb{R}^N$, so there is a set of $N-1$ linearly independent vectors that span the plane of possible solutions. Any such set can be made into an orthonormal basis,

$$Q = [\vec{e}_1, \vec{e}_2, ..., \vec{e}_{N-1}] \tag{3.12}$$

where the $\vec{e}_i \in \mathbb{R}^N$ are column basis vectors. Each of these basis vectors is a complementary solution of equation 3.11 satisfying

$$\sum_{i=1}^{N} s_i = 0. \tag{3.13}$$

Assuming that Q is generated numerically from a set of vectors that do not satisfy orthonormality, it is likely that there will be small numerical errors associated with the orthonormalization. To prevent cascading errors, all vector components less that 10^{-10} will be set to 0. Given that the components of a size distribution vector

will be on the order of 10^0 or 10^1, anything less than 10^{-10} can be reasonably treated as numerical 0.

Any point on the plane can now be expressed as the sum of a linear combination of the $\vec{e_i}$ and any particular solution to equation 11. In other words, if we have a feasible solution $\vec{s_0}$ that is a valid size distribution, i.e. a size distribution that adds up to 100%, we can get to any other valid size distribution via:

$$\vec{s_0} + Q\vec{\delta}, \tag{3.14}$$

where $\vec{\delta}$ is a vector of dimension $N-1$ that satisfies $Q\vec{\delta} = \vec{0}$.

Additionally, because the basis set is orthonormal, a gradient may be calculated via finite differences with N function evaluations; one for the point where the gradient is being evaluated, and N-1 perturbations for each orthogonal degree of freedom. Orthonormality also means that the magnitude of the gradient can be easily found, making the iterative method described by equation 3.10 viable. This formulation ensures that as long as $\vec{x_c}$ in equation 3.10 is a valid set of calibration parameters, $\vec{x_n}$ will be as well. The scalar Shield's Number can augment the distribution vector to make a single calibration vector, or its gradient and step size can be calculated separately.

If stochastic optimization proves necessary, randomized feasible solutions may be generated using equation 3.14. Given a known feasible solution, randomizing the components of $\vec{\delta}$ will provide a random set of feasible solutions. Changing the distribution from which the random values are drawn can produce a cloud of feasible solutions around an initial vector $\vec{s_0}$.

3.5 Conclusion

In this work, a modification to the EKF algorithm was presented for dynamic recalibration of process-based models and real-time assimilation of data. An environmental application, sediment transport, was proposed and the implementation of the method for the specific problem described. Due to a the absence of needed boundary condition data, the method was not tested on this sediment transport model but rather on a simple pendulum and a set of synthetically constructed data and measurements. Assimilation of the data through the proposed method results in convergence of the estimates for calibration variables over time.

The results provide motivation for further study given the potential power of the successful application of the algorithm to real-world applications. It would provide the means to provide system predictions prior to having sufficient calibration data, automatically calibrate the model, and automatically adjust calibration to outlier events should they occur. Given the proliferation of data collection and sensor technology, a framework for intelligently integrating large quantities and varieties of data into existing process-based modeling techniques will be key to successfully extracting the information content of this data.

References

Gary W. Brunner. *HEC-RAS River Analysis System User's Manual*. US Army Corps of Engineers Institute for Water Resources Hydrologic Engineering Center, 609 Second Street Davis, CA 95616-4687, February 2016.

Joel Franklin. *Computational Methods for Physics*. Cambridge University Press, 2013.

Scott D. Hamshaw. Suspended sediment prediction using artificial neural networks and local hydrometeorological data. Master's thesis, University of Vermont, 2014.

J.J. McDonnell, M. Sivapalan, K. Vache, S. dunn, G. grant, R. Haggerty, C. Hinz, R. Hooper, J. Kirchner, M. L. Roderick, J. Selker, and M. Weiler. Moving beyond heterogeneity and prcoess complexity: A new vision for watershed hydrology. *Water Resources Research*, 43(7), 2007.

David J. Neelin, Annalisa Bracco, Luo Hao, James C. McWilliams, and Joyce E. Meyerson. Considerations for parameter optimization and sensitivity in climate models. *Proceedings of the National Academy of Sciences of the United States of America*, 107(50):21349–21354, 2010.

Darren S. Olsen, Brett B. Roper, Jeffrey L. Kershner, Richard Henderson, and Eric Archer. Sources of variability in conducting pebble counts: Their potential influcence on the results of stream monitoring programs. *Journal of the American Water Resources Association*, 41(5):1225–1236, October 2005.

Alexander Szalay and Jim Gray. 2020 computing: Science in an exponential world. *Nature*, 440(7083):413–414, 2006.

Chapter 4

Overall Conclusions

Conclusions Process-based models provide valuable information and understanding in a diverse array of applications; the embedding of *a priori* knowledge of internal system dynamics means that evaluations of system responses to different conditions can, implicitly or explicitly, have that information embedded, as well. Advances in computing power, and the increased availability of data for calibration these models, have allowed for modeling of phenomena on temporal and spatial scales that in the not-to-distant past would have been unimaginable. Continent wide hydrologic modeling on a 1-km scale, including surface water routing and infiltration, soil moisture, and meteorological effects, is available. Weather forecasting is reaching unprecedented levels of accuracy, in large part due to improved process-based multi-phase fluid dynamics models based on the underlying physics.

These advancements have masked a fundamental philosophical question about the use and applicability of process-based models and process-based modeling: does an uncalibrated model that does not match observed outcomes for a given system and scenario contain any useful information about the system, or is its use merely a computational exercise? In other words, does a model have to match a real-world

scenario to within some tolerance for it to be useful? The methods and experiments presented in this thesis are based on the belief that merely the physics embedded in the model contains useful information whether the scenario being modeled represents the real world precisely, and whether the model is calibrated, or not.

In Chapter 2, a method was presented for the combined use of HEC-RAS version 4.1, a surface water model using heuristic multi-objective optimization. In this thesis, the application of interest was bridge scour at a particular bridge in Vermont, for which a model had been built, calibrated and validated by a local engineering firm. For the purpose of this work, the initial model geometry was modified to reflect a scenario that does not reflect the real-world, and would not be implemented in any way. The initial HEC-RAS model condition represented, more or less, a return to minimum floodplain access that is not being considered and is not realistic from an engineering or practical standpoint. This fact is the first departure from the state of current practice and research: the model was constructed not as a hypothetical scenario, but to elucidate the behavior of a certain facet of the system.

That behavior of interest in Chapter 2 is the response of bridge scour to floodplain access at locations up and downstream of the (fixed) bridge location. This explicit examination of floodplain access impact on bridge scour is absent in the literature. Numerical optimization of a constructed cost function was then used to assess the relative sensitivity of floodplain access with respect to bridge scour at different locations. This sensitivity analysis was performed using the relative ranking of the optimal decision variables. The interpretation of optimization results as sensitivity, rather than assessing sensitivity of a cost function to changes in decision variables near the optimum, is a new use of numerical optimization in engineering applications.

Despite the possibility that 2-D modeling would be more appropriate for the study site and test model, the results of the sensitivity analysis should be robust to

more detailed modeling efforts. The analysis pointed to downstream locations as most salient, a finding supported by the hydraulics of the site. The reach is relatively short, providing insufficient volume in floodplains to mitigate flood waves. Physical variables at the bridge, such as velocity, are controlled by a backwater caused by downstream constriction rather than the attenuation of flood waves by upstream floodplains. In addition to identifying only one cross section (and two decision variables) as salient, multiple weightings of the two objectives (minimal floodplain access and minimal scour) resulted in the same ranking of the optimal values of these variables. This is a key finding, as it provides a means for stakeholders to obtain information that helps guide decision-making without having to explicitly weight the multiple competing objectives initially.

In Chapter 3, a framework is provided for a more comprehensive approach to modeling sediment transport in rivers and streams. Process-based modeling provided by HEC-RAS is again used, and under the proposed framework this model is not calibrated prior to use. This use of an un-calibrated model in a data-assimilation algorithm is novel. The Extended Kalman Filter is one such possible algorithm for dynamically recalibrating the model to the assimilated system states, which depend in part on the uncalibrated model predictions. This last step depends on, and assumes that, information about the state is contained in model outputs even prior to thorough calibration. Successful implementation of this kind of framework would have wide implications in the age of big-data, allowing massive amounts of data to be combined with models and update on a real-time basis our beliefs and estimates about underlying physical parameters. It is analogous to a Bayesian approach and would permit calibration to be flexible to new information, rather than fixed to past observations.

A synthetic system is proposed to validate the framework described above. A

simple pendulum system and a numerical method with a small time-step are used to generate a set of true system states. Noise is added, and a numerical method with a larger time step used as the model. Both the traditional pre-calibration, as well as the novel dynamic calibration method were performed, and the performance of the filtered state estimates were compared to the true states. Prediction of the dynamic calibration and EKF algorithm had good agreement with true states, and dynamic calibration resulted in convergence of the best estimate of the pendulum length to its true value. The performance of the method on the synthetic system shows that it is worthy of future study; the description of its potential application to sediment transport demonstrates its portability to real-world modeling problems for which it is well-suited and fills a need. Both of these projects used process-based models as parts of a larger modeling framework for decision support and to improve models and the utilization of data. This is not new. Both chapter introductions and in the literature review document the coupling of process-based models with numerical optimization for optimal management of environmental problems and decision support tools going back decades. Assimilation of large amounts of data into with process based models is likewise not a new technique, and has been used for many environmental applications including sediment transport modeling. Standard practices for using models for these kinds of applications exist for good reason. In many case, it is fair to reject the use of an uncalibrated model as a computational exercise or to question the wisdom of modeling a scenario that no one is proposing.

What is novel about the methods and results described in this thesis is that they show that relaxing these requirements can be useful in some applications. Intelligent modification of a site model can allow evaluation of the behavior and response of particular phenomena, guiding future modeling efforts and engineering design choices. The sensitivity analysis presented here for the bridge site could, for example, prevent

time and money being spent on a complex 2-D model of a reach too short for upstream floodplain access to have any role, not to mention the real decision-support information provided by the sensitivity analysis as a stand-alone. The data assimilation method, meanwhile, provides a means for treating data on a real time basis as evidence for modifiable calibration parameters. These parameters can act as fudge factors than strictly physical values, and so a flexible means of adjusting them in real-time is useful even if it means breaking the taboo of using an uncalibrated model. In both projects, leveraging the information content of the model itself independent of the individual site or observed data, was key to developing the methods and providing new insights, modeling techniques, and decision-support tools for hydraulic, hydrologic, and environmental problems.

Bibliography

Ian A. Anderson, Mandar M. Dewoolkar, Donna M. Rizzo, and Dryver R. Huston. Scour related vermont bridge damage from tropical storm irene. In *Structures Congresss*, pages 505–515, 2014.

L.A. Arneson, L.W. Zevenbergen, P.F. Lagasse, and P.E. Clopper. Evaluating scour at bridges. Technical report, National Highway Institute, 2012.

Charles Berenbrock and Andrew W. Tranmer. Simulation of flow, sediment transport, and sediment mobility of the lower coeur d'alene river, idaho. Scientific Investigations Report 2008-5093, U.S. Geological Survey, 2008. Table 7.

Jean-Louis Briaud, Paolo Gardoni, and Congpu Yao. Statistical, risk, and reliability analysis of bridge scour. *Journal of Geotechnical and Geoenvironmental Engineering*, 2(140), 2014.

Gary W. Brunner. *HEC-RAS River Analysis System User's Manual*. US Army Corps of Engineers Institute for Water Resources Hydrologic Engineering Center, 609 Second Street Davis, CA 95616-4687, February 2016a.

Gary W. Brunner. Hec-rhec-ras river analysis system hydraulic reference manual. Technical report, US Army Corps of Engineers Institute for Water Resources Hydrologic Engineering Center, February 2016b.

A.H. Cardoso and R. Bettess. Effects of time and channel geometry on scour at bridge abutments. *Journal of Hydraulic Engineering*, 125(4):388–399, April 1999.

Yee-Meng Chiew. Scour and scour countermeasures at bridge sites. *Transactions of Tianjin University*, 14(4):289–295, 2008.

Larry M. Deschaine, Theodore P. Lillys, and Janos D. Pinter. Groundwater remediation design using physics-based flow, transport and optimizatioin technologies. *Environmental Systems Research*, 2(6), May 2013.

Margaret J. Eppstein. *Efficient Data Inversion for Large Multi-Dimensional Problems Using an Approximate Extended Kalman filter with Data Driven Zonation*. PhD thesis, University of Vermont, 1997.

Joel Franklin. *Computational Methods for Physics*. Cambridge University Press, 2013.

Christopher Goodell. *Breaking the HEC-RAS Code: A User's Guide to Automating HEC-RAS*. h2ls, 2014.

Scott D. Hamshaw. Suspended sediment prediction using artificial neural networks and local hydrometeorological data. Master's thesis, University of Vermont, 2014.

Gregory S. Hornby, Jason D. Lohn, and Derek S. Linden. Computer-automated evolution of an x-band antenna for nasa's space technology 5 mission. *Evolutionary Computation*, 19(1):1–23, 2011.

Peggy A. Johnson, Richard D. Hey, Eric R. Brown, and David L. Rosgen. Stream restoration in the vicinity of bridges. *Journal of the American Water Resources Association*, 38(1):55, February 2002.

Kyunghyun Kim, Minji Park, Joong-Hyuk Min, Ingu Ryu, Mi-Ri Kang, and Lan Joo Park. Simulation of algal bloom dynamics in a river with the ensemble kalman filter. *Journal of Hydrology*, 519:2810–2821, 2014.

R.D. Kouchakzadeh, S. an dTownsend. Maximum scour depth at bridge abutments terminating in the floodplain zone. *Canadian Journal of Civil Engineering*, 24(1): 996–1006, 1997.

Michael P. Lamb, William E. Dietrich, and Jeremy G. Venditti. Is the critical shields stress for incipient sediment motion dependent on channel-bed slope? *Journal of Geophysical Research: Earth Surface*, 113(F2), 2008. ISSN 2156-2202.

Fang-Fang Li, Christine A. Schoemaker, Jun Qiu, and Jia-Hua Wei. Hierarchical multi-reservoir optimization modmodel for real-world complexity with application to the three gorges system. *Environmental Modeling and Software*, 69:319–329, 2015.

Zhiqiang Li. Applications using the ordinary and extended kalman ffilter to characterize groundwater contaminant sources. Master's thesis, University of Vermont, 2007.

Cheng-Dar Liou, Kuo-Hsiung Wang, and Meng-Wei Liou. Genetic algorithm to the machine repair problem with two removable servers operating under the triadic (0, q, n, m) policy. *Applied Mathematical Modelling*, 37(1819):8419 – 8430, 2013. ISSN 0307-904X.

G. Mesfin and M. Shuhaimi. A chance constrained approach for a gas processing plant with uncertain feed conditions. *Computers & Chemical Engineering*, 34(8): 1256 – 1267, 2010. ISSN 0098-1354.

Arezoo Rafieein Nasab, Dong-Jun Seo, Haksu Lee, and Sunghee Kim. Comparitive evaluation of maximum likelihood ensemble filter and ensemble kalman filter for real-time assimilation of stream data into operational hydrologic models. *Journal of Hydrology*, 519:2663–2675, 2014.

David J. Neelin, Annalisa Bracco, Luo Hao, James C. McWilliams, and Joyce E. Meyerson. Considerations for parameter optimization and sensitivity in climate models. *Proceedings of the National Academy of Sciences of the United States of America*, 107(50):21349–21354, 2010.

Darren S. Olsen, Brett B. Roper, Jeffrey L. Kershner, Richard Henderson, and Eric Archer. Sources of variability in conducting pebble counts: Their potential influcence on the results of stream monitoring programs. *Journal of the American Water Resources Association*, 41(5):1225–1236, October 2005.

Gerardo M. E. Perillo and J. William Lavelle. Sediment transport processes in estuaries: An introduction. *Journal of Geophysical Research*, 94(C10):14,287–14,288, October 1989.

Ryan P. Rossell and Francis C. K. Ting. Hydraulic and contraction scour analysis of a meandering channel: james river bridges near mitchell, south dakota. *Journal of Hydraulic Engineering*, 13(2):1286–1296, December 2013.

Jos Samuel, Paulin Coulibaly, Gift Dumedah, and Hamid Moradkhani. Assessing model state and forecasts variation in hydrologic data assimilation. *Journal of Hydrology*, 513:127–141, 2014.

D.M. Sheppard, B. Melville, and H. Demir. Evaluation of existing equations for local scour at bridge piers. *Journal of Hydraulic Engineering*, 140(1):14–23, 2014.

Shahar Shlomi, Avi Ostfeld, Hillel Rubin, and Christine Shoemaker. Optimal groundwater contamination monitoring using pumping wells. *Water Science and Technology*, 62(3):556–569, 2010.

Rainer Storn and Kenneth Price. Differential evolution – a simple and efficient heuristic for global optimization over continuous spaces. *Journal of Global Optimization*, 11:341–359, 1997.

Terry W. Sturm and Nazar Sadiq Janjua. Clear-water scour around abutments in floodplains. *Journal of Hydraulic Engineering*, 120(8):956–972, August 1994.

Appendix A

Use of the HEC-RAS API

HEC-RAS is a software package developed and distributed by the United States Army Corps of Engineers-Hydrologic Engineering Center (USACE-HEC). It can model streams and rivers and has support for many hydraulic structures including bridges, damns, weirs, levees, and storage areas, and it can perform steady state or transient flow simulations. Version 4.1 can perform steady-state sediment transport calculations, and Version 5.0 has extended those capabilities to include transient sediment transport modeling. It is widely used in both the public and private sectors, and is one of the few programs accepted by FEMA for flood insurance studies.

Its predecessor, HEC-2, operated by reading in text files and writing output text files – there was no graphical interface. HEC-RAS, in contrast, is used via a GUI. While there is an API for the program contained in a dynamic link library file, until recently there was no documentation for this functionality, and the possibilities offered by automated control of the program remain relatively unexplored (Goodell, 2014). The API is needed because, while HEC-RAS model parameters are set in input text files, the output files are binary and can only be read by HEC-RAS, and extracted using its internal functions via the API.

The process of using the API to set HEC-RAS model parameters, run simulations, and extract and post-process results was done using Python. HEC-RAS models are specified in a set of text files, and code was written to automatically modify these text files to specify model geometry and floodplain encroachment values. HEC-RAS was run using an API function call. Output data, which is stored in binary files, was likewise extracted using an API function. Once simulation results were extracted into the Python routine, post-processing was performed.

The API could be similarly used for the unvalidated sediment transport application. Sediment model parameters are set in hdf5 files, which can be edited and read from Python. Running simulations and extracting results would require substantively the same procedures for an unsteady sediment transport model as the unsteady hydraulic model did.